INSTITUTE OF PHYSICS PUBLISHING INVERSE PROBLEMS

Inverse Problems **20** (2004) 507–532 PII: S0266-5611(04)66670-6

Synthetic-aperture imaging through a dispersive layer

Margaret Cheney[1] **and Clifford J Nolan**[2]

[1] Department of Mathematical Sciences, Rensselaer Polytechnic Institute, Troy, NY 12180, USA
[2] Department of Mathematics and Statistics, University of Limerick, Republic of Ireland

Received 24 July 2003, in final form 22 January 2004
Published 27 February 2004
Online at stacks.iop.org/IP/20/507 (DOI: 10.1088/0266-5611/20/2/013)

Abstract
This paper develops a method for forming a synthetic-aperture image of a flat surface seen through a homogeneous layer of a material that is dispersive, i.e., its wave speed varies with frequency. We outline first a simplified scalar model for electromagnetic wave propagation in a dispersive medium; the resulting equation could also be used for acoustics. We show that the backscattered signal can be viewed as a Fourier integral operator applied to the ground reflectivity function. The reconstruction method, which is based on backprojection, can be used for arbitrary sensor paths and corrects for the radiated beam pattern, the source waveform and geometrical spreading factors. The method correctly reconstructs the singularities (such as edges) that are visible from the sensor.

1. Introduction

This paper is motivated by the problem of synthetic-aperture radar (SAR) imaging of forested areas. Most of the foliage-penetrating radar systems [29, 49, 50] are airborne and use frequencies in the range 10 MHz–1 GHz, which correspond to wavelengths between 30 m and 30 cm. At these relatively long wavelengths, models for wave propagation through foliage generally take the form of homogenized effective medium models [6, 15, 31, 48].

Some of the foliage-penetrating radar systems, moreover, are ultrawideband: the frequency band for the Swedish CARABAS system [49], for example, is 20–90 MHz, and for the GeoSAR system [50] is 270–430 MHz. Over such a wide relative bandwidth, some of the effective medium models predict a variation in the complex permittivity by as much as 50%. This raises the issue of how to account for the dispersion (i.e., variation of propagation speed with frequency) in the image formation process. The goal of the paper is to address this issue.

In this paper, we consider the effect of dispersion on the formation of synthetic-aperture images. We use the simplest possible example of a dispersive layer, namely a flat, homogeneous, dispersive layer over a flat surface. Ultimately, of course, this is much too simple to model real foliage, but it provides a beginning for the study of imaging through a dispersive medium. In particular, the theory developed in this paper could also be applied to imaging through materials such as soil [1, 51] and human tissue [1].

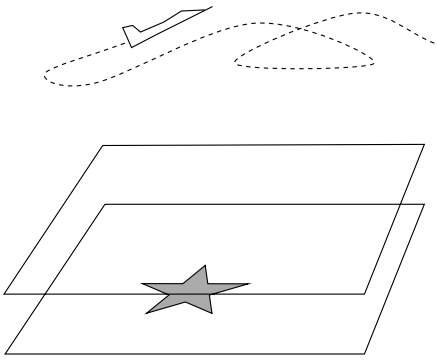

Figure 1. Data collection geometry. The star represents a feature in the scene to be imaged, and the region between the planes is filled by a homogeneous dispersive material.

For this simple model, we are able to obtain an explicit imaging formula and a corresponding point spread function that can be used to evaluate the image. Extensions to more complicated (known) geometry can probably be made by combining the approach of [5] with geometrical optics for dispersive media [27].

The paper begins in section 2 with a detailed discussion of a simplified scalar mathematical model for the received signal. This is followed, in section 3, by analysis of the received signal under certain general conditions on the nature of the dispersion. In particular, we show that the received signal can be expressed as a Fourier integral operator (FIO) applied to the scene. For this FIO, we find, in section 4, an approximate inverse; this inverse provides the imaging formula. The paper concludes with some appendices containing technical details.

2. The mathematical model

Our goal in this section is to derive a mathematical expression for the received radar signal. We model the scatterers of interest as variations in the ground reflectivity function supported on a plane. For scattering from this plane we use a single-scattering (Born) approximation. The dispersive layer is modelled as a (known) homogeneous dispersive half-space in which the plane of unknown reflectivity is embedded. This model ignores multiple scattering between the plane (ground) and the top of the dispersive layer (the foliage crown); we assume such effects have been subtracted out of the data.

We assume that the sensor (antenna) moves along a path γ that is well separated from the top (at $x_3 = H$) of the dispersive half-space. We assume that the path is smooth; it is otherwise arbitrary, and for example would be allowed to perform loops and self-intersections (see figure 1).

Waves emanate from the sensor and are received back at the same sensor. We make the start–stop approximation, i.e., we neglect motion of the sensor during the measurement, and we neglect issues related to the discreteness of the pulses.

Derivation of the mathematical model involves (1) a scalar model for wave propagation, (2) a model for the field emanating from an antenna, (3) a model for the wave after it propagates through a homogeneous dispersive layer and (4) a model for scattering from the earth.

2.1. The equations

For SAR, the correct model is Maxwell's equations, which we write as

$$\nabla \times \boldsymbol{E} = -\partial_t \boldsymbol{B}, \tag{1}$$

$$\nabla \times \boldsymbol{H} = \boldsymbol{J} + \partial_t \boldsymbol{D}, \tag{2}$$

$$\nabla \cdot \boldsymbol{D} = \rho, \tag{3}$$

$$\nabla \cdot \boldsymbol{B} = 0. \tag{4}$$

Here $\boldsymbol{E}$ is the electric field, $\boldsymbol{H}$ the magnetic field, $\boldsymbol{D}$ the electric displacement, $\boldsymbol{B}$ the magnetic induction, $\boldsymbol{J}$ the current density and ρ the charge density. The four fields $\boldsymbol{E}, \boldsymbol{D}, \boldsymbol{H}, \boldsymbol{B}$ are related by constitutive relations, which in this paper we assume to be of the form [25]

$$\boldsymbol{B}(t, \boldsymbol{x}) = \mu_0 \boldsymbol{H}(t, \boldsymbol{x}), \tag{5}$$

$$\boldsymbol{D}(t, \boldsymbol{x}) = \int_0^\infty \varepsilon(s, \boldsymbol{x}) \boldsymbol{E}(t - s, \boldsymbol{x}) \, \mathrm{d}s \equiv (\varepsilon *_t \boldsymbol{E})(t, \boldsymbol{x}). \tag{6}$$

Here μ_0 is the magnetic permeability of free space, which means that we are considering non-magnetic materials. The relation between $\boldsymbol{D}$ and $\boldsymbol{E}$ is a causal convolution in time with the electric permittivity ϵ. In general, the permittivity kernel is of the form $\varepsilon(s, \boldsymbol{x}) = \epsilon_\infty(\boldsymbol{x})\delta(s) + \chi(s, \boldsymbol{x})$ with χ being smooth; ϵ_∞ is called the *instantaneous response* or *optical response* and χ is called the *susceptibility kernel*. Discontinuities in the electric and magnetic fields propagate with speed $c(\boldsymbol{x}) = 1/(\mu_0 \epsilon_\infty(\boldsymbol{x}))^{1/2}$.

If we use (5) and (6) to eliminate $\boldsymbol{B}$ and $\boldsymbol{D}$ in (1) and (2), and then substitute the curl of (1) into (2), we obtain

$$\nabla \times \nabla \times \boldsymbol{E} = -\partial_t \mu_0 \boldsymbol{J} - \partial_{tt}(\mu_0 \varepsilon *_t \boldsymbol{E}). \tag{7}$$

Finally, we use the identity $\nabla \times \nabla \times \boldsymbol{E} = \nabla(\nabla \cdot \boldsymbol{E}) - \nabla^2 \boldsymbol{E}$ to write (7) as

$$\nabla^2 \boldsymbol{E} - \partial_{tt}(\mu_0 \varepsilon *_t \boldsymbol{E}) - \nabla(\nabla \cdot \boldsymbol{E}) = \mu_0 \partial_t \boldsymbol{J}. \tag{8}$$

Up to this point, our only assumptions have been (5) and (6); we now make a simplifying assumption to reduce (8) to three uncoupled scalar equations.

Assumption 1. We assume that $\nabla(\nabla \cdot \boldsymbol{E}) = 0$; this reduces (8) to

$$\nabla^2 \boldsymbol{E} - \partial_{tt}(\mu_0 \varepsilon *_t \boldsymbol{E}) = \mu_0 \partial_t \boldsymbol{J}. \tag{9}$$

Assumption 1 does not hold in general; instead, from (3) and (6) we should have $\nabla \cdot (\varepsilon *_t \boldsymbol{E}) = \rho$. However, (9) holds within a homogeneous medium in which there are no free charges, and in particular it holds for wave propagation in air and within a homogeneous dispersive layer. In general (9) does not hold at interfaces between materials; at such interfaces there is coupling between the different components of E [23]. By using (9), we are ignoring such coupling, and we are thus ignoring polarization effects. Consequently we consider only one component of (9), thus reducing the problem to a scalar one.

Because electromagnetic waves are rapidly attenuated in the earth, we assume that the (non-dispersive) scattering takes place in a thin region near the surface. We use the superscript 0 to designate points on the earth's surface, e.g. $(\boldsymbol{x}_T, x_3^0)$ and $(\boldsymbol{z}_T, z_3^0)$.

Assumption 2. The permittivity kernel is of the form $\varepsilon(s, \boldsymbol{x}) = V(\boldsymbol{x}_T)\delta(x_3 - x_3^0)\delta(s) + \epsilon_0 \varepsilon_r(s, \boldsymbol{x})$, where $\boldsymbol{x}_T = (x_1, x_2)$, where ε_r and x_3^0 are known, ϵ_0 denotes the permittivity of free space and where V is unknown. The dispersive layer extends to $x_3 = H > x_3^0$. We assume that the sensor path γ is well above $x_3 = H$.

Here V, the *ground reflectivity function*, is the quantity we wish to reconstruct.

The case in which the earth's surface is not flat was considered, for the non-dispersive case, in [37], which used techniques similar to those used in this paper.

With the notation of assumption 2, we write our wave equation as the single scalar equation

$$\nabla^2 E - \partial_{tt}\big(c_0^{-2}\varepsilon_r *_t E\big) + (V\delta)\partial_{tt}E = -j_s, \tag{10}$$

where $c_0 = 1/(\mu_0\epsilon_0)^{1/2}$ and where j_s denotes one component of $-\mu_0\partial_t \boldsymbol{J}$ in (9). In (10), ε_r is assumed known but V is unknown.

2.2. Sources in and above a dispersive half-space

In this subsection, we obtain an explicit representation for the half-space Green's function g, which satisfies

$$\nabla^2 g(t, \boldsymbol{x}, \boldsymbol{y}) - \partial_{tt}\big(c_0^{-2}\varepsilon_r *_t g\big)(t, \boldsymbol{x}, \boldsymbol{y}) = -\delta(t)\delta(\boldsymbol{x} - \boldsymbol{y}). \tag{11}$$

Our derivation follows the appendix of [8].

We take the Fourier transform (11) in t, which results in

$$(\nabla^2 + k^2\epsilon_r(\omega, x_3))G(\omega, \boldsymbol{x}, \boldsymbol{y}) = -\delta(\boldsymbol{x} - \boldsymbol{y}), \tag{12}$$

where we have written $k = \omega/c_0$ and $\epsilon_r = \epsilon/\epsilon_0$ with ϵ being the temporal Fourier transform of ε. We consider the case in which

$$\epsilon_r(\omega, x_3) = \begin{cases} 1, & \text{for} \quad x_3 > H \\ \epsilon_r^-(\omega), & \text{for} \quad x_3 < H. \end{cases} \tag{13}$$

Because the medium does not vary in the x_1 and x_2 directions, G is of the form $G(\omega, \boldsymbol{x}, \boldsymbol{y}) = G(\omega, x_1 - y_1, x_2 - y_2, x_3, y_3)$.

Finally we take the Fourier transform (12) also in the horizontal variables x_1 and x_2, which results in

$$\big(\partial_{x_3}^2 + k^2\eta_3^2(\omega, \boldsymbol{\eta}_T, x_3)\big)\hat{G}(\omega, \boldsymbol{\eta}_T, x_3, y_3) = -\delta(x_3 - y_3), \tag{14}$$

where we have written the variables dual to x_1 and x_2 in scaled form as $k\boldsymbol{\eta}_T = (k\eta_1, k\eta_2)$, and where $\eta_3^2(\omega, \boldsymbol{\eta}_T, x_3) = \epsilon_r(\omega, x_3) - |\boldsymbol{\eta}_T|^2$.

Equation (14) can be solved explicitly [8] in our half-space case (13). In particular, away from $x_3 = y_3$, the general solution of (14) is, for $x_3 > H$,

$$\hat{G}^+(\omega, \boldsymbol{\eta}_T, x_3, y_3) = A^+(\omega, \boldsymbol{\eta}_T, y_3)\,\mathrm{e}^{\mathrm{i}k\eta_3^+(x_3 - H)} + B^+(\omega, \boldsymbol{\eta}_T, y_3)\,\mathrm{e}^{-\mathrm{i}k\eta_3^+(x_3 - H)}, \tag{15}$$

and, for $x_3 < H$,

$$\hat{G}^-(\omega, \boldsymbol{\eta}_T, x_3, y_3) = A^-(\omega, \boldsymbol{\eta}_T, y_3)\,\mathrm{e}^{\mathrm{i}k\eta_3^-(x_3 - H)} + B^-(\omega, \boldsymbol{\eta}_T, y_3)\,\mathrm{e}^{-\mathrm{i}k\eta_3^-(x_3 - H)}, \tag{16}$$

where

$$\eta_3^+(\omega, \boldsymbol{\eta}_T) = \begin{cases} \sqrt{1 - |\boldsymbol{\eta}_T|^2}, & \text{for} \quad 1 > |\boldsymbol{\eta}_T| \\ \mathrm{i}(\operatorname{sgn} k)\sqrt{|\boldsymbol{\eta}_T|^2 - 1}, & \text{for} \quad 1 < |\boldsymbol{\eta}_T|, \end{cases} \tag{17}$$

and

$$\eta_3^-(\omega, \boldsymbol{\eta}_T) = \sqrt{\epsilon_r^-(\omega) - |\boldsymbol{\eta}_T|^2}, \tag{18}$$

the branch of the square root being chosen so that the imaginary part of η_3^- is positive when $\omega \geqslant 0$ and negative when $\omega < 0$. For $|\boldsymbol{\eta}_T| < 1$, η_3^+ is real; if $|\boldsymbol{\eta}_T| > 1$, η_3^+ is purely imaginary. This latter case gives rise to evanescent waves, which decay exponentially in the direction of propagation. We note that η_3^- can be complex even for small $|\boldsymbol{\eta}_T|$. We define the vectors $\boldsymbol{\eta}^\pm = \big(\boldsymbol{\eta}_T, \eta_3^\pm\big)$, which satisfy $\boldsymbol{\eta}^\pm \cdot \boldsymbol{\eta}^\pm = \epsilon_r$.

The coefficients $A^\pm$ and $B^\pm$ of (15) and (16) depend on whether the source height y_3 is greater than or less than H and on whether x_3 is greater than or less than H and y_3. When x_3 is

greater than both H and y_3, the condition that $\hat{g}$ be upgoing implies that B^+ is zero; when x_3 is less than both H and y_3, the condition that $\hat{g}$ be downgoing implies that A^- is zero. $\hat{G}$ and its x_3 derivatives are continuous except at $x_3 = y_3$, where $\hat{G}$ is continuous but its x_3 derivative jumps by minus one. Solving for the A and B in both cases results in the following. For $y_3 > H$, we have [8]

$$\hat{G}(\omega, \boldsymbol{\eta}_T, x_3, y_3) = \frac{\mathrm{i}}{2k\eta_3^+} \begin{cases} R\left(\eta_3^+, \eta_3^-\right) \mathrm{e}^{\mathrm{i}k\eta_3^+(x_3+y_3-2H)} + \mathrm{e}^{\mathrm{i}k\eta_3^+|x_3-y_3|}, & \text{for} \quad x_3 > H \\ T\left(\eta_3^+, \eta_3^-\right) \mathrm{e}^{\mathrm{i}k\eta_3^+(y_3-H)}\, \mathrm{e}^{\mathrm{i}k\eta_3^-(H-x_3)}, & \text{for} \quad x_3 < H, \end{cases} \tag{19}$$

and for $y_3 < H$, we have

$$\hat{G}(\omega, \boldsymbol{\eta}_T, x_3, y_3) = \frac{\mathrm{i}}{2k\eta_3^-} \begin{cases} T\left(\eta_3^-, \eta_3^+\right) \mathrm{e}^{\mathrm{i}k\eta_3^-(H-y_3)}\, \mathrm{e}^{\mathrm{i}k\eta_3^+(x_3-H)}, & \text{for} \quad x_3 > H \\ \mathrm{e}^{\mathrm{i}k\eta_3^-|x_3-y_3|} + R\left(\eta_3^-, \eta_3^+\right) \mathrm{e}^{-\mathrm{i}k\eta_3^-(x_3+y_3-2H)}, & \text{for} \quad x_3 < H, \end{cases} \tag{20}$$

where

$$T(\lambda_1, \lambda_2) = \frac{2\lambda_2}{\lambda_1 + \lambda_2}, \tag{21}$$

and

$$R(\lambda_1, \lambda_2) = \frac{\lambda_2 - \lambda_1}{\lambda_1 + \lambda_2}. \tag{22}$$

Note that since the imaginary parts of $k\eta_3^+$ and $k\eta_3^-$ are non-negative, the exponents in (19) and (20) are decaying.

In order to model the field received at the antenna, we need the field transmitted through the layer from a source (the antenna) above the layer, and the field from a source (due to scattering) on the ground that is transmitted through the layer and received at the antenna. We denote these components by $\hat{G}^{\downarrow}$ and $\hat{G}^{\uparrow}$; more precisely they are the second line of (19) and the first line of (20), respectively. The resulting frequency-domain Green's functions are

$$G^{\downarrow}(\omega, \boldsymbol{x}, \boldsymbol{y}) = \frac{1}{(2\pi)^2} \int \frac{\mathrm{i}T\left(\eta_3^+, \eta_3^-\right)}{2k\eta_3^+} \mathrm{e}^{\mathrm{i}k\boldsymbol{\eta}_T\cdot(\boldsymbol{x}_T-\boldsymbol{y}_T)}\, \mathrm{e}^{\mathrm{i}k\eta_3^+(y_3-H)}\, \mathrm{e}^{\mathrm{i}k\eta_3^-(H-x_3)} k^2\, \mathrm{d}^2\boldsymbol{\eta}_T, \tag{23}$$

$$G^{\uparrow}(\omega, \boldsymbol{x}, \boldsymbol{y}) = \frac{1}{(2\pi)^2} \int \frac{\mathrm{i}T\left(\eta_3^-, \eta_3^+\right)}{2k\eta_3^-} \mathrm{e}^{\mathrm{i}k\boldsymbol{\eta}_T\cdot(\boldsymbol{x}_T-\boldsymbol{y}_T)}\, \mathrm{e}^{\mathrm{i}k\eta_3^-(H-y_3)}\, \mathrm{e}^{\mathrm{i}k\eta_3^+(x_3-H)} k^2\, \mathrm{d}^2\boldsymbol{\eta}_T. \tag{24}$$

The time-domain Green's function is recovered from its Fourier transform by

$$g(t, \boldsymbol{x}, \boldsymbol{y}) = \frac{1}{(2\pi)^3} \int \mathrm{e}^{\mathrm{i}k\boldsymbol{\eta}_T\cdot(\boldsymbol{x}_T-\boldsymbol{y}_T)-\mathrm{i}\omega t}\, \hat{G}(\omega, \boldsymbol{\eta}_T, x_3, y_3)\, \mathrm{d}\omega\, k^2\, \mathrm{d}^2\boldsymbol{\eta}_T. \tag{25}$$

Thus, for example, the field at the point $\boldsymbol{x}$ on the earth's surface due to a point source at $\boldsymbol{y}$ above the dispersive layer is

$$g^{\downarrow}(t, \boldsymbol{x}, \boldsymbol{y}) = \frac{1}{(2\pi)^3} \int \frac{\mathrm{i}T\left(\eta_3^+, \eta_3^-\right)}{2k\eta_3^+} \mathrm{e}^{\mathrm{i}k\boldsymbol{\eta}_T\cdot(\boldsymbol{x}_T-\boldsymbol{y}_T)-\mathrm{i}\omega t}\, \mathrm{e}^{\mathrm{i}k\eta_3^+(y_3-H)}\, \mathrm{e}^{\mathrm{i}k\eta_3^-(H-x_3)}\, \mathrm{d}\omega\, k^2\, \mathrm{d}^2\boldsymbol{\eta}_T, \tag{26}$$

where we have used (23). If we add and subtract the quantity $\boldsymbol{\eta}_T \cdot \boldsymbol{x}_T$ in the phase of (26), and use the notation $\boldsymbol{\eta}_{\downarrow}^{\pm} = \left(\boldsymbol{\eta}_T, -\eta_3^{\pm}\right)$ and $\boldsymbol{x}^H = (\boldsymbol{x}_T, H)$, we see that (26) involves a product of the plane waves $\exp[\mathrm{i}\, k\boldsymbol{\eta}_{\downarrow}^+ \cdot (\boldsymbol{x}^H - \boldsymbol{y})]$ and $\exp[\mathrm{i}\, k\boldsymbol{\eta}_{\downarrow}^- \cdot (\boldsymbol{x} - \boldsymbol{x}^H)]$, which correspond to propagation in the upper medium from $\boldsymbol{y}$ to the intermediate point $\boldsymbol{x}^H$ and propagation in the lower medium from $\boldsymbol{x}^H$ to $\boldsymbol{x}$, respectively.

We note that models with more layers can be accommodated by using a multiple-layer Green's function [24].

2.3. The field emanating from an antenna

In the preceding section, we have obtained an explicit expression for the Green's function for a dispersive half-space. This Green's function corresponds to a source of the form $\delta(t)\delta(\boldsymbol{x}-\boldsymbol{y})$.

The antenna, however, is not a point source [52] $\delta(\boldsymbol{x})$, and the signal sent to the antenna is not a delta function $\delta(t)$. Therefore to obtain a simple antenna model, we replace $\delta(t)\delta(\boldsymbol{x})$ of (11) by $j_s(t,\boldsymbol{x})$ of (10).

Typical antennas used for foliage-penetrating radar are horns, microstrip arrays [45], broadband dipoles [22] and log-periodic arrays of dipoles [17]. For the case of dipoles, j_s can be taken proportional to (the time derivative of) the current density on the dipole; for a horn or slotted waveguide, j_s is often taken to be an effective current density over the aperture.

We write j_s in terms of its Fourier transform J_s:

$$j_s(t,\boldsymbol{x}) = \frac{1}{2\pi}\int \mathrm{e}^{-\mathrm{i}\omega t} J_s(\omega,\boldsymbol{x})\,\mathrm{d}\omega, \tag{27}$$

where ω denotes the angular frequency. In practice, the waveform j_s is such that only a certain interval $[\omega_{\min},\omega_{\max}]$ contributes significantly to (27); we call this set the *effective support* of J_s. The difference $(\omega_{\max}-\omega_{\min})$ is the (angular-frequency) *bandwidth*. The fact that j_s is bandlimited means that ultimately we reconstruct bandlimited approximations to singular components of the coefficient V.

The field E^{in} emanating from the antenna then satisfies

$$\nabla^2 E^{\mathrm{in}}(t,\boldsymbol{x}) - \partial_{tt}\big(c_0^{-2}\varepsilon_r *_t E^{\mathrm{in}}\big)(t,\boldsymbol{x}) = -j_s(t,\boldsymbol{x}), \tag{28}$$

so that

$$\begin{aligned} E^{\mathrm{in}}(t,\boldsymbol{x}) &= \int g^{\downarrow}(t-t',\boldsymbol{x}_T-\boldsymbol{y}_T,x_3,y_3)\,j_s(t,\boldsymbol{y})\,\mathrm{d}t'\,\mathrm{d}\boldsymbol{y} \\ &= \int \mathrm{e}^{-\mathrm{i}\omega t} G^{\downarrow}(\omega,\boldsymbol{x}_T-\boldsymbol{y}_T,x_3,y_3)\,J_s(\omega,\boldsymbol{y})\,\mathrm{d}\omega\,\mathrm{d}\boldsymbol{y}. \end{aligned} \tag{29}$$

We write $\boldsymbol{y}=\boldsymbol{\gamma}(s)+\boldsymbol{q}$, where $\boldsymbol{\gamma}(s)$ denotes the centre of the antenna. Then, using (23) in (29), we have

$$\begin{aligned} E^{\mathrm{in}}(t,s,\boldsymbol{x},s) = \frac{1}{(2\pi)^3}\int \frac{\mathrm{i}T\big(\eta_3^+,\eta_3^-\big)}{2k\eta_3^+}\,\mathrm{e}^{\mathrm{i}k\boldsymbol{\eta}_T\cdot(\boldsymbol{x}_T-\boldsymbol{\gamma}_T(s))-\mathrm{i}\omega t}\,\mathrm{e}^{\mathrm{i}k\eta_3^+(\gamma_3(s)-H)}\,\mathrm{e}^{\mathrm{i}k\eta_3^-(H-x_3)} \\ \times \tilde{J}_s(\omega,s,\boldsymbol{\eta}_T)\,\mathrm{d}\omega\,k^2\,\mathrm{d}^2\boldsymbol{\eta}_T, \end{aligned} \tag{30}$$

where

$$\tilde{J}_s(\omega,s,\boldsymbol{\eta}_T) = \int \mathrm{e}^{-\mathrm{i}k(\boldsymbol{\eta}_T\cdot\boldsymbol{q}_T-\eta_3^+q_3)}\,J_s(\omega,\boldsymbol{\gamma}(s)+\boldsymbol{q})\,\mathrm{d}\boldsymbol{q}, \tag{31}$$

is an approximation to the antenna beam pattern.

We note that in reality, the antenna beam pattern is strongly affected by the vector nature of the current and the vector structure of Maxwell's equations. Approximation (31) can be used to give a good approximation to the size of the main lobe of the beam pattern, but does not necessarily provide an accurate model for the overall beam pattern.

2.4. A linearized scattering model

We write $E=E^{\mathrm{in}}+E^{\mathrm{sc}}$ in (10) and use (28) to obtain

$$\nabla^2 E^{\mathrm{sc}} - \partial_{tt}\big(c_0^{-2}\varepsilon_r *_t E^{\mathrm{sc}}\big) = -(V\delta)\partial_t^2 E. \tag{32}$$

We recall that the reflectivity function V contains all the information about how the medium differs from the background. It is V, or at least its discontinuities and other singularities, that we want to recover.

We can write (32) as an integral equation [33]

$$E^{\mathrm{sc}}(t,\boldsymbol{x}) = -\int g^{\uparrow}(t-\tau,\boldsymbol{x}_T-\boldsymbol{z}_T,x_3,z_3)V(\boldsymbol{z}_T)\delta\big(z_3-z_3^0\big)\partial_\tau^2 E(\tau,\boldsymbol{z})\,\mathrm{d}\tau\,\mathrm{d}\boldsymbol{z}. \tag{33}$$

A commonly used approximation [21, 28], often called the *Born approximation* or the *single-scattering approximation*, is to replace the full field E on the right-hand side of (33) and (32) by the incident field E^{in}, which converts (33) to

$$\begin{aligned} E^{\mathrm{sc}}(t,\boldsymbol{x}) &\approx E_B^{\mathrm{sc}}(t,\boldsymbol{x},s) \\ &:= -\int g^{\uparrow}(t-\tau,\boldsymbol{x}_T-\boldsymbol{z}_T,x_3,z_3)V(\boldsymbol{z}_T)\delta\big(z_3-z_3^0\big)\partial_\tau^2 E^{\mathrm{in}}(\tau,s,\boldsymbol{z},s)\,\mathrm{d}\tau\,\mathrm{d}\boldsymbol{z}, \end{aligned} \tag{34}$$

where the subscript B reminds us that we are using the Born approximation. The value of this approximation is that it removes the nonlinearity in the inverse problem: it replaces the product of two unknowns (V and E) by a single unknown (V) multiplied by the known incident field.

The Born approximation makes the problem simpler, but it is not necessarily a good approximation. Another linearizing approximation that can be used for reflection from smooth surfaces is the *Kirchhoff approximation*, in which the scattered field is replaced by its geometrical optics approximation at the surface of the scatterer [5, 28]. Here, however, we consider only the Born approximation.

In summary, we assume

Assumption 3. The data S are *linearly* related to V, i.e., we use a single-scattering (Born) approximation.

In (34) we substitute (30) and (24) (with $\boldsymbol{\eta}$ replaced by $\boldsymbol{\mu}$) and simplify the result by carrying out the τ integration and one of the ω integrations:

$$\begin{aligned} E_B^{\mathrm{sc}}(t,\boldsymbol{x},s) = \frac{1}{(2\pi)^5}\int &\frac{\mathrm{i}T\big(\mu_3^-,\mu_3^+\big)}{2k\mu_3^-}\,\mathrm{e}^{\mathrm{i}k\boldsymbol{\mu}_T\cdot(\boldsymbol{x}_T-\boldsymbol{z}_T)-\mathrm{i}\omega t}\,\mathrm{e}^{\mathrm{i}k\mu_3^-(H-z_3)}\,\mathrm{e}^{\mathrm{i}k\mu_3^+(x_3-H)} \\ &\times V(\boldsymbol{z}_T)\delta\big(z_3-z_3^0\big)\omega^2\frac{\mathrm{i}T\big(\eta_3^+,\eta_3^-\big)}{2k\eta_3^+}\,\mathrm{e}^{\mathrm{i}k\boldsymbol{\eta}_T\cdot(\boldsymbol{z}_T-\boldsymbol{\gamma}_T(s))}\,\mathrm{e}^{\mathrm{i}k\eta_3^-(H-z_3)} \\ &\times \mathrm{e}^{\mathrm{i}k\eta_3^+(\gamma_3(s)-H)}\,\tilde{J}_s(\omega,s,\boldsymbol{\eta}_T)\,\mathrm{d}\omega\,k^4\,\mathrm{d}^2\boldsymbol{\mu}_T\,\mathrm{d}^2\boldsymbol{\eta}_T\,\mathrm{d}\boldsymbol{z}, \end{aligned} \tag{35}$$

where $\mu_3^{\pm}$ are defined as in (17) and (18).

We note that physically, the full scattered field involves a reflection from the top of the foliage as well as a reflection from the ground beneath the foliage. This foliage-crown bounce is not included in E^{sc} because it is part of the (assumed known) incident wave. In other words, we are assuming that the foliage-crown bounce has been subtracted out; E^{sc} involves only scattering from the ground.

2.5. The received signal

We model reception of the field (35) by the antenna by writing $\boldsymbol{x} = \boldsymbol{\gamma}(s) + \boldsymbol{q}$ in (35), and calculating

$$S(t,s) = \int E_B^{\mathrm{sc}}(t-t',\boldsymbol{\gamma}(s)+\boldsymbol{q},s)\,j_r(t',\boldsymbol{\gamma}(s),\boldsymbol{q})\,\mathrm{d}t'\,\mathrm{d}\boldsymbol{q}, \tag{36}$$

where j_r denotes the reception pattern for the antenna. For an array antenna, for example, j_r would be the (possibly complex) weighting with respect to which the signals from the different

elements are combined. Generally the reception pattern is the same as the transmission pattern j_s.

We obtain

$$S(t,s) = \frac{-1}{(2\pi)^5} \int \frac{T\left(\mu_3^-, \mu_3^+\right)}{2k\mu_3^-} \mathrm{e}^{\mathrm{i}k\boldsymbol{\mu}_T\cdot(\boldsymbol{\gamma}_T(s)-\boldsymbol{z}_T)-\mathrm{i}\omega t} \mathrm{e}^{\mathrm{i}k\mu_3^-(H-z_3^0)} \mathrm{e}^{\mathrm{i}k\mu_3^+(\gamma_3(s)-H)}$$
$$\times V(\boldsymbol{z}_T)\tilde{J}_r(\omega, s, \boldsymbol{\mu}^+)\omega^2 \frac{T\left(\eta_3^+, \eta_3^-\right)}{2k\eta_3^+} \mathrm{e}^{\mathrm{i}k\boldsymbol{\eta}_T\cdot(\boldsymbol{z}_T-\boldsymbol{\gamma}_T(s))} \mathrm{e}^{\mathrm{i}k\eta_3^-(H-z_3^0)}$$
$$\times \mathrm{e}^{\mathrm{i}k\eta_3^+(\gamma_3(s)-H)} \tilde{J}_s(\omega, s, \boldsymbol{\eta}_T)\, \mathrm{d}\omega\, k^4\, \mathrm{d}^2\boldsymbol{\mu}_T\, \mathrm{d}^2\boldsymbol{\eta}_T\, \mathrm{d}\boldsymbol{z}_T, \tag{37}$$

where $\tilde{J}_r$ is defined in the same way as $\tilde{J}_s$.

Technical difficulties arise from evanescent waves, for which $\eta_3^\pm$ or $\mu_3^\pm$ is purely imaginary, and from horizontally propagating waves, for which $\eta_3^\pm = 0$ or $\mu_3^\pm = 0$. The contribution to the data from evanescent waves, however, is negligible, because assumption 2 implies that terms such as $\exp\left(\mathrm{i}\, k\eta_3\left(z_3^0 - H\right)\right)$ are exponentially small. The contributions from horizontally propagating waves are also negligible, because such waves cannot travel between the antenna and the scatterer.

Assumption 4. We neglect contributions from evanescent and horizontally propagating waves.

We therefore insert into (37) a smooth cutoff function $\psi(\omega, \boldsymbol{\eta}_T, \boldsymbol{\mu}_T)$ that restricts the domain of integration to be strictly within the set $\{|\boldsymbol{\eta}_T|, |\boldsymbol{\mu}_T| < \min\{1, \epsilon_r(\omega)\}\}$. The cutoff ψ must be chosen so that all its derivatives decay faster than any polynomial.

The idealized inverse problem is to determine V from knowledge of S for $t \in (T_1, T_2)$ and for s on some interval $(s^{\min}, s^{\max})$.

A number of technical difficulties arise if we attempt to image points directly underneath the antenna [37]. In particular, we will see that our imaging algorithm cannot be used for data coming from locations directly underneath the current location of the antenna. We therefore make the following assumption.

Assumption 5. At every position $\boldsymbol{\gamma}(s)$ on the (smooth) flight path, the height $\gamma_3(s)$ and the time $T_1(s)$ at which data recording begins are related by $T_1(s) > T_0 > 2\left|\gamma_3(s) - x_3^0\right|/c_0$ for some T_0.

The abrupt ends of the curve γ tend to cause artefacts in the image; consequently, it is useful to multiply the data by a smooth taper function $m(s,t)$ which is zero outside $(s^{\min}, s^{\max}) \times (T_1, T_2)$. Consequently, we write the data as

$$d(t,s) = m(s,t)S(t, \boldsymbol{\gamma}(s))$$
$$= \frac{m(s,t)}{(2\pi)^5} \int \frac{\mathrm{i}T\left(\mu_3^-, \mu_3^+\right)}{2k\mu_3^-} \mathrm{e}^{\mathrm{i}k\boldsymbol{\mu}_T\cdot(\boldsymbol{\gamma}_T(s)-\boldsymbol{z}_T)-\mathrm{i}\omega t} \mathrm{e}^{\mathrm{i}k\mu_3^-(H-z_3^0)} \mathrm{e}^{\mathrm{i}k\mu_3^+(\gamma_3(s)-H)}$$
$$\times V(\boldsymbol{z}_T)\tilde{J}_r(\omega, s, \boldsymbol{\mu}^+) \frac{\mathrm{i}T\left(\eta_3^+, \eta_3^-\right)}{2k\eta_3^+} \mathrm{e}^{\mathrm{i}k\boldsymbol{\eta}_T\cdot(\boldsymbol{z}_T-\boldsymbol{\gamma}_T(s))} \mathrm{e}^{\mathrm{i}k\eta_3^-(H-z_3^0)} \mathrm{e}^{\mathrm{i}k\eta_3^+(\gamma_3(s)-H)}$$
$$\times \tilde{J}_s(\omega, s, \boldsymbol{\eta}_T)\psi(\omega, \boldsymbol{\eta}_T, \boldsymbol{\mu}_T)\omega^2\, \mathrm{d}\omega\, k^4\, \mathrm{d}^2\boldsymbol{\mu}_T\, \mathrm{d}^2\boldsymbol{\eta}_T\, \mathrm{d}_T^2\boldsymbol{z}. \tag{38}$$

3. Analysis of the received signal

Our goal in this section is to write the model for the data (38) in the form of an FIO [10, 19, 44] and then use FIO theory to analyse it. In order to do this, we need certain conditions on the

dispersion properties of the intermediate layer. These conditions are satisfied by the Debye and Lorentz models, and also by some, but not all, dispersion models developed specifically to model foliage.

Assumptions about the dispersion are necessary because the model for the data (38) is not presently written in the form of an FIO: the phase involves a complicated dependence on the internal variables, namely the temporal frequency ω and the scaled spatial frequencies $\boldsymbol{\mu}_T$ and $\boldsymbol{\eta}_T$. The phase of an FIO must be homogeneous of degree 1 in these variables. For the scaled spatial frequency variables $\boldsymbol{\mu}_T$ and $\boldsymbol{\eta}_T$, there is an easy remedy: we make the change of variables $\boldsymbol{\eta}_T = \tilde{\boldsymbol{\eta}}_T/\omega$ and $\boldsymbol{\mu}_T = \tilde{\boldsymbol{\mu}}_T/\omega$.

The dependence on ω, however is more complicated: ω occurs in the functions μ_3^- and η_3^- through their dependence on $\epsilon_r(\omega)$. The dependence of ϵ_r on ω is not arbitrary: from (6) we know that the Fourier transform of ϵ_r is zero on the negative real (time) axis, and therefore by the Paley–Wiener theorem [42], ϵ_r must be analytic in the upper half-plane. Moreover, smoothness in the time domain implies large-ω decay of $\epsilon_r - \epsilon_\infty$ of at least $O(\omega^{-1})$ [23]. This latter fact enables us to simplify the phase of (38) by reassigning parts of μ_3^- and η_3^- to the amplitude.

Assumption 6. We assume that $\epsilon_r(\omega)$ is of the form

$$\epsilon_r(\omega) = \epsilon_\infty + \epsilon_s(\omega), \tag{39}$$

where $\epsilon_s(\omega)$ satisfies

$$\partial_\omega^\beta \epsilon_s(\omega) \leqslant C_\beta (1+\omega^2)^{-(1+|\beta|)/2}, \tag{40}$$

for every non-negative integer β.

We give examples below of specific models, some of which satisfy this assumption and some of which do not.

The large-ω decay of ϵ_s implies that ϵ_s appears only in the remainder terms of large-ω asymptotic calculations. In order to exploit this fact, we write $\eta_3^-(\omega, \boldsymbol{\eta}_T) = \sqrt{\epsilon_r^-(\omega) - |\boldsymbol{\eta}_T|^2}$ as

$$\eta_3^-(\omega, \boldsymbol{\eta}_T) = \eta_\infty(\boldsymbol{\eta}_T) + \eta_a(\omega, \boldsymbol{\eta}_T), \tag{41}$$

where $\eta_\infty(\boldsymbol{\eta}_T) = \sqrt{\epsilon_\infty - |\boldsymbol{\eta}_T|^2}$ and

$$\eta_a(\omega, \boldsymbol{\eta}_T) = \eta_3^-(\omega, \boldsymbol{\eta}_T) - \eta_\infty(\boldsymbol{\eta}_T). \tag{42}$$

We define μ_a similarly.

We will include the remainder term $\exp\big(\mathrm{i}\, k \eta_a(\omega, \boldsymbol{\eta}_T)\big(z_3^0 - H\big)\big)$ in the amplitude, thus removing it from the phase of (38). This enables us to replace η^- and μ^-, which depend on ω, by η_∞^- and μ_∞^-, which do not.

3.1. Specific models for dispersion

Examples of models that do and do not satisfy assumption 6 are given below. High-frequency decay rates must be faster than ω^{-1} for time-domain continuity [23], but some of the phenomenological models do not satisfy this condition.

3.1.1. Fung–Ulaby model (8–17 GHz). The model of Fung and Ulaby [15] for the effective permittivity of leafy vegetation is based on a model for the permittivity of the leaf material together with a mixing model.

If ν is the fractional volume occupied by leaves, then the effective relative permittivity of the foliage is

$$\epsilon_r(\omega) = \epsilon_\infty + \frac{a_1 - \mathrm{i}a_2}{1 + b^2\omega^2}, \tag{43}$$

where $\epsilon_\infty = 5.5\nu + (1 - \nu)$, $a_1 = (51.56\nu_w - 0.5)\nu$ with ν_w being the water volume fraction within a typical leaf, $a_2 = a_1 b$, and b is an empirical factor involving the temperature-dependent relaxation time for water. At 20 °C, we have roughly $b = 185/(2\pi c_0)$.

The Fung–Ulaby model satisfies assumption 6.

3.1.2. Brown–Curry model (100 MHz–10 GHz). The Brown–Curry model [6] is a model for a sparse random medium such as the branches and tree trunks of a forest. A modification due to Ding [11] of the Brown–Curry model is

$$\epsilon_r(\omega) = \left[\epsilon_\infty + \frac{b}{1 + (\omega/\omega_c)^2}\right] + \mathrm{i}\left[\frac{(\omega/\omega_c)b}{1 + (\omega/\omega_c)^2} + \frac{a}{(2\pi\omega)^{0.96}}\right]. \tag{44}$$

Here $\epsilon_\infty \approx 4.5$, b is a constant that depends on the density and fractional volume of wood, $a = 1.5 \times 10^9$ (respectively 4×10^9) when the electric field is parallel (perpendicular) to the wood grain and $2\pi\omega_c$ is a temperature-dependent frequency that is roughly 20 GHz at 25 °C.

The Brown–Curry model does *not* quite satisfy assumption 6, because the last term of (44) decays slightly more slowly than ω^{-1}.

3.1.3. Debye model. The Debye model is generally good for polar molecules such as water in the microwave regime. The Debye model is

$$\epsilon_r(\omega) = \epsilon_\infty + \frac{\epsilon_s - \epsilon_\infty}{1 - \mathrm{i}\omega\tau}, \tag{45}$$

where for water, typical values are as follows. The zero-frequency relative permittivity is $\epsilon_s = 80.35$, the infinite-frequency relative permittivity is $\epsilon_\infty = 1.00$ and the relaxation time is $\tau = 8.13$ ps [41].

The Debye model satisfies assumption 6.

3.1.4. Lorentz model. The Lorentz model, which is a harmonic-oscillator model, is generally good for solid materials. The permittivity for a Lorentz medium is given by

$$\epsilon_r(\omega) = \epsilon_\infty - \frac{b^2}{\omega^2 - \omega_0^2 + 2\mathrm{i}\omega\delta}, \tag{46}$$

where ϵ_∞ is real and positive.

The Lorentz model satisfies assumption 6.

3.2. The forward operator is an FIO

We write (38) as the map $F : V \mapsto d$. We write F in the form of an FIO by making the change of variables $\boldsymbol{\eta}_T = \tilde{\boldsymbol{\eta}}_T/\omega$ and $\boldsymbol{\mu}_T = \tilde{\boldsymbol{\mu}}_T/\omega$ and by moving η_a^- and μ_a^- from the phase into the amplitude:

$$FV(s,t) = \int \mathrm{e}^{\mathrm{i}\phi(t,s,\boldsymbol{x},\omega,\tilde{\boldsymbol{\mu}}_T,\tilde{\boldsymbol{\eta}}_T)} A(t, s, \boldsymbol{x}, \omega, \tilde{\boldsymbol{\mu}}_T, \tilde{\boldsymbol{\eta}}_T) V(\boldsymbol{x}_T)\, \mathrm{d}^2\tilde{\mu}_T\, \mathrm{d}^2\tilde{\boldsymbol{\eta}}_T\, \mathrm{d}\omega\, \mathrm{d}^2\boldsymbol{x}_T, \tag{47}$$

where

$$\phi(t, s, \boldsymbol{x}, \omega, \tilde{\boldsymbol{\mu}}_T, \tilde{\boldsymbol{\eta}}_T) = -\omega\Bigg(t - \Bigg[\frac{\tilde{\boldsymbol{\mu}}_T}{\omega} \cdot (\gamma_T(s) - \boldsymbol{x}_T) + \tilde{\mu}_\infty\big(H - x_3^0\big) + \tilde{\mu}_3^+(\gamma_3(s) - H) + \frac{\tilde{\boldsymbol{\eta}}_T}{\omega} \cdot (\boldsymbol{x}_T - \gamma_T(s)) + \tilde{\eta}_\infty\big(H - x_3^0\big) + \tilde{\eta}_3^+(\gamma_3(s) - H)\Bigg] \Big/ c_0\Bigg), \tag{48}$$

where $\tilde{\mu}_3^+ = \mu_3^+(\omega, \tilde{\boldsymbol{\mu}}_T/\omega)$, and $\tilde{\eta}_3^+$, $\tilde{\mu}_\infty$ and $\tilde{\eta}_\infty$ are defined similarly, and

$$A(t, s, \boldsymbol{x}, \omega, \tilde{\boldsymbol{\mu}}_T, \tilde{\boldsymbol{\eta}}_T) = -\frac{m(s,t)}{(2\pi)^5} \frac{T\big(\tilde{\mu}_3^-, \tilde{\mu}_3^+\big)}{2k\tilde{\mu}_3^-} \mathrm{e}^{\mathrm{i}k\tilde{\mu}_a^-(H - x_3^0)} \tilde{J}_r(\omega, s, \tilde{\boldsymbol{\mu}}_T/\omega) \times \frac{T\big(\tilde{\eta}_3^+, \tilde{\eta}_3^-\big)}{2k\tilde{\eta}_3^+} \mathrm{e}^{\mathrm{i}k\tilde{\eta}_a^-(H - x_3^0)} \tilde{J}_s(\omega, s, \tilde{\boldsymbol{\eta}}_T/\omega)\psi(\omega, \tilde{\boldsymbol{\eta}}_T/\omega, \tilde{\boldsymbol{\mu}}_T/\omega). \tag{49}$$

The following proposition shows that moving η_a from the phase to the amplitude is legitimate, because the resulting amplitude satisfies the conditions for being in the *symbol class* S^0 of order 0 (and type $(1, 0)$).

Proposition 1. *For every triple of non-negative integers $\boldsymbol{\beta} = (\beta_1, \beta_2, \beta_3)$,*

$$\tilde{a}(\omega, \tilde{\boldsymbol{\eta}}_T) = a(\omega, \tilde{\boldsymbol{\eta}}_T/\omega) = \psi(\omega, \tilde{\boldsymbol{\eta}}_T/\omega)\, \mathrm{e}^{\mathrm{i}k\tilde{\eta}_a(\omega, \tilde{\boldsymbol{\eta}}_T/\omega)(H - z_3^0)}, \tag{50}$$

satisfies

$$\big|\partial_{\tilde{\eta}_1}^{\beta_1} \partial_{\tilde{\eta}_2}^{\beta_2} \partial_\omega^{\beta_3} \tilde{a}(\omega, \tilde{\boldsymbol{\eta}}_T)\big| \leqslant C_\beta(1 + |(\omega, \tilde{\boldsymbol{\eta}}_T)|^2)^{-|\boldsymbol{\beta}|/2} = \tilde{C}_\beta(1 + \omega^2)^{-|\boldsymbol{\beta}|/2}; \tag{51}$$

i.e., a is in S^0. A similar estimate holds if $\boldsymbol{\eta}_T$ is replaced by $\boldsymbol{\mu}_T$.

The proof of this proposition is given in appendix A.

We now make an assumption about the antenna beam patterns. This assumption is satisfied, for example by a broadband antenna (i.e., $\tilde{J}_r$ and $\tilde{J}_s$ are approximately independent of ω over the effective bandwidth). Mathematically, this assumption ensures that F is an FIO.

Assumption 7. The antenna activation patterns $\tilde{J}_r$ and $\tilde{J}_s$ each satisfy, for some m,

$$\sup_{s \in K} \big|\partial_s^\alpha \partial_\omega^{\beta_0} \partial_{\tilde{\boldsymbol{\eta}}}^{\boldsymbol{\beta}} J(\omega, s, \tilde{\boldsymbol{\eta}}_T)\big| \leqslant C(1 + \omega^2 + |\tilde{\boldsymbol{\eta}}|^2)^{[m - (\beta_0 + |\boldsymbol{\beta}|)]/2}, \tag{52}$$

where $\partial_{\tilde{\eta}}^{\boldsymbol{\beta}} = \partial_{\tilde{\eta}_1}^{\beta_1} \partial_{\tilde{\eta}_2}^{\beta_2}$, $|\tilde{\boldsymbol{\eta}}|^2 = |\tilde{\eta}_1|^2 + |\tilde{\eta}_2|^2$, $|\boldsymbol{\beta}| = \beta_1 + \beta_2$, where K is any compact subset of $\mathbb{R}_\omega \times (s^{\min}, s^{\max}) \times \mathbb{R}^2_{\tilde{\eta}}$, and the constant C depends on K, α, β_0, β_1, β_2 and β.

In other words, we assume that both the $\tilde{J}$s are in the same symbol class S^m. This assumption can be weakened to admit other symbol classes [10, 19].

With this assumption we have the following estimate.

Proposition 2. *Suppose assumptions 1–7 are satisfied. Then for some m,*

$$\sup_{(s,t,x) \in K} \big|\partial_s^{\alpha_s} \partial_t^{\alpha_t} \partial_{(x_1,x_2)}^{(\alpha_1,\alpha_2)} \partial_\omega^{\beta_0} \partial_{(\tilde{\eta}_1,\tilde{\eta}_2)}^{(\beta_1,\beta_2)} \partial_{(\tilde{\mu}_1,\tilde{\mu}_2)}^{(\beta_3,\beta_4)} A(t, s, \boldsymbol{x}, \omega, \tilde{\boldsymbol{\mu}}_T, \tilde{\boldsymbol{\eta}}_T)\big| \leqslant C(1 + |\omega|^2 + |\tilde{\boldsymbol{\eta}}|^2 + |\tilde{\boldsymbol{\mu}}|^2)^{(m - |\boldsymbol{\beta}|)/2}, \tag{53}$$

where $|\boldsymbol{\beta}| = \sum_{i=0}^4 |\beta_i|$, $|\boldsymbol{\alpha}| = |\alpha_s| + |\alpha_t| + |\alpha_1| + |\alpha_2|$, where K is any compact subset of $\mathbb{R}_t \times (s^{\min}, s^{\max}) \times \mathbb{R}^2_{\boldsymbol{x}_T} \times \mathbb{R}_\omega \times \mathbb{R}^2_{\tilde{\mu}} \times \mathbb{R}^2_{\tilde{\eta}}$, and the constant C depends on K and on the α and β.

Proof. A is a product of symbols and is thus again a symbol [19]. The only potential difficulty is zeros of $\tilde{\mu}_3^\pm$ and $\tilde{\eta}_3^\pm$, but these have been excluded by assumption 4 via the smooth cutoff function ψ. □

Corollary 1. *Under assumptions 1–7, F is an FIO.*

Proof. The phase function is homogeneous of degree 1 in the vector of internal ('frequency') variables $(\omega, \tilde{\boldsymbol{\mu}}_T, \tilde{\boldsymbol{\eta}}_T)$. The phase function is real valued, and on the effective support of the amplitude A, $\partial\phi/\partial t = \omega$ never vanishes. □

3.3. Analysis of the forward operator

3.3.1. The critical set. The main contributions to F come from the critical points of the phase, i.e., from the set of points $(s, t, x, \omega, \tilde{\boldsymbol{\mu}}_T, \tilde{\boldsymbol{\eta}}_T)$ satisfying

$$\begin{aligned} 0 = \partial_\omega \phi = -\Bigg(t - \Bigg[& \frac{\tilde{\boldsymbol{\mu}}_T}{\omega} \cdot (\boldsymbol{\gamma}_T(s) - \boldsymbol{x}_T) + \tilde{\mu}_\infty\big(H - x_3^0\big) + \tilde{\mu}_3^+(\gamma_3(s) - H) \\ & + \frac{\tilde{\boldsymbol{\eta}}_T}{\omega} \cdot (\boldsymbol{x}_T - \boldsymbol{\gamma}_T(s)) + \tilde{\eta}_\infty\big(H - x_3^0\big) + \tilde{\eta}_3^+(\gamma_3(s) - H)\Bigg] \Big/ c_0\Bigg) \\ & - \omega^{-2} \sum_{i=1}^{2} \big(\partial_{\tilde{\mu}_i}\phi + \partial_{\tilde{\eta}_i}\phi\big), \end{aligned} \tag{54}$$

$$0 = \partial_{\tilde{\mu}_i}\phi = -\frac{1}{c_0}\left[(\gamma_i(s) - x_i) - \frac{\tilde{\mu}_i/\omega}{\tilde{\mu}_\infty}\big(H - x_3^0\big) - \frac{\tilde{\mu}_i/\omega}{\tilde{\mu}_3^+}(\gamma_3(s) - H)\right], \tag{55}$$

$$0 = \partial_{\tilde{\eta}_i}\phi = -\frac{1}{c_0}\left[(x_i - \gamma_i(s)) - \frac{\tilde{\eta}_i/\omega}{\tilde{\eta}_\infty}\big(H - x_3^0\big) - \frac{\tilde{\eta}_i/\omega}{\tilde{\eta}_3^+}(\gamma_3(s) - H)\right], \tag{56}$$

for $i = 1, 2$. We note that (55) and (56) imply that the term with the summation sign in (54) vanishes.

Geometrical interpretation of the critical set. We will see below that equation (54) says that the travel time t is the sum of the travel times along the upgoing and downgoing paths from $\gamma(s)$ to x. The equations for these paths are equations (55) and (56).

Equations (55) and (56) can be written as

$$\begin{aligned} \frac{\gamma_1(s) - x_1}{\mu_1} &= \frac{\gamma_2(s) - x_2}{\mu_2} = \frac{\gamma_3(s) - H}{\mu_3^+} + \frac{H - x_3^0}{\mu_\infty}, \\ \frac{\gamma_1(s) - x_1}{\eta_1} &= \frac{\gamma_2(s) - x_2}{\eta_2} = \frac{\gamma_3(s) - H}{-\eta_3^+} + \frac{H - x_3^0}{-\eta_\infty}. \end{aligned} \tag{57}$$

We will see below that these equations express Snell's law for a ray refracting through the interface at $x_3 = H$.

A line with direction $\boldsymbol{\mu}_\downarrow^+$ through the point $\boldsymbol{\gamma}(s)$ will intersect the plane $x_3 = H$ at a certain point (see figure 2), which we denote by $\boldsymbol{x}^H = \big(x_1^H, x_2^H, H\big)$. We write $\boldsymbol{\mu}^\infty = (\mu_1, \mu_2, \mu_\infty)$, $\boldsymbol{\mu}_\downarrow^\infty = (\mu_1, \mu_2, -\mu_\infty)$ and similarly for $\boldsymbol{\eta}$.

Proposition 3 (Geometrical interpretation of (57))**.** *On the critical set,* $-\boldsymbol{\mu}^+ = \boldsymbol{\eta}_\downarrow^+ = (\widehat{\boldsymbol{x}^H - \boldsymbol{\gamma}(s)})$ *and* $-\boldsymbol{\mu}^\infty = \boldsymbol{\eta}_\downarrow^\infty = \epsilon_\infty(\widehat{\boldsymbol{x} - \boldsymbol{x}^H})$. *The first and second lines of (57) therefore describe the same refracting ray path.*

The second equation of (57) therefore corresponds to a ray that starts at $\boldsymbol{\gamma}(s)$ with direction vector $\boldsymbol{\eta}_\downarrow^+ = \big(\eta_1, \eta_2, -\eta_3^+\big)$, travels in direction $\boldsymbol{\eta}_\downarrow^+$ until it hits the interface $x_3 = H$ at the point $\boldsymbol{x}^H$, and continues, now with direction vector $\boldsymbol{\eta}_\downarrow^\infty$, to the point $\boldsymbol{x}$ on the surface $x_3 = x_3^0$. The first equation of (57) corresponds to a ray that traces the same path in the opposite direction.

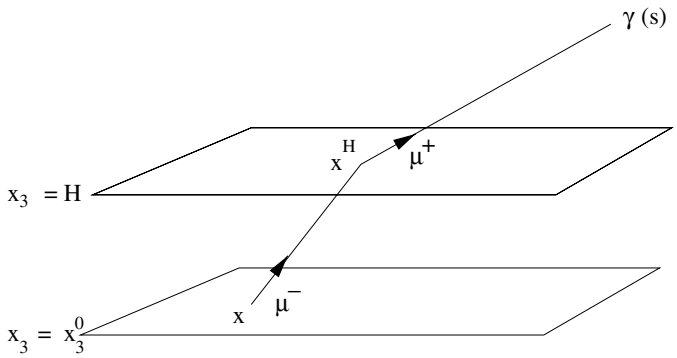

Figure 2. The geometry of the critical set. On the critical set, $\boldsymbol{\mu}^- = \boldsymbol{\mu}^\infty$, $\boldsymbol{\eta}_\downarrow^+ = -\boldsymbol{\mu}^+$, and $\boldsymbol{\eta}_\downarrow^- = \boldsymbol{\eta}_\downarrow^\infty = -\boldsymbol{\mu}^\infty$.

Proof of proposition 3. The first equation of (57) contains two pieces of information: first, the equation

$$\frac{\gamma_1(s) - y_1}{\mu_1} = \frac{\gamma_2(s) - y_2}{\mu_2} = \frac{\gamma_3(s) - H}{\mu_3^+} + \frac{H - y_3}{\mu_\infty}, \tag{58}$$

describes a geometrical set of points $\boldsymbol{y} = (y_1, y_2, y_3)$. Second, (57) says that the point $\boldsymbol{x} = \left(x_1, x_2, x_3^0\right)$ lies in this geometrical set.

First we consider the set of points $\boldsymbol{y}$ satisfying (58). If $\boldsymbol{y} = \boldsymbol{y}^H = \left(y_1^H, y_2^H, H\right)$, we see that (58) reduces to

$$\frac{\gamma_1(s) - y_1^H}{\mu_1} = \frac{\gamma_2(s) - y_2^H}{\mu_2} = \frac{\gamma_3(s) - H}{\mu_3^+}, \tag{59}$$

which, if we denote the common ratio of (59) by ρ^H, can be written in vector form as $\boldsymbol{y}^H = \boldsymbol{\gamma}(s) - \rho^H \boldsymbol{\mu}^+$. This says that a point $\boldsymbol{y}^H = \left(y_1^H, y_2^H, H\right)$ lies on the line with direction vector $\boldsymbol{\mu}^+$ through $\boldsymbol{\gamma}(s)$. Since $\boldsymbol{\mu}^+ \cdot \boldsymbol{\mu}^+ = 1$, and, by assumption 4, $\boldsymbol{\mu}^+$ is real, $\boldsymbol{\mu}^+$ must be equal to $\widehat{\boldsymbol{\gamma}(s) - \boldsymbol{y}^H}$ or its negative. In fact, since the third components of $\widehat{\boldsymbol{\gamma}(s) - \boldsymbol{y}^H}$ and $\boldsymbol{\mu}^+$ are both positive, we must have $\boldsymbol{\mu}^+ = \widehat{\boldsymbol{\gamma}(s) - \boldsymbol{y}^H}$.

If we now add and subtract y_1^H/μ_1 and y_2^H/μ_2 in the first and second members of (58), respectively, we obtain

$$\frac{\gamma_1(s) - y_1^H}{\mu_1} + \frac{y_1^H - y_1}{\mu_1} = \frac{\gamma_2(s) - y_2^H}{\mu_2} + \frac{y_2^H - y_2}{\mu_2} = \frac{\gamma_3(s) - H}{\mu_3^+} + \frac{H - y_3}{\mu_\infty}; \tag{60}$$

subtracting (59) from (60) results in the equations for a line with direction vector $\boldsymbol{\eta}^\infty$ joining $\boldsymbol{y}^H$ to a point $\boldsymbol{y}$:

$$\frac{y_1^H - y_1}{\mu_1} = \frac{y_2^H - y_2}{\mu_2} = \frac{H - y_3}{\mu_\infty}; \tag{61}$$

or, if we denote the common ratio of (60) by ρ and carry out the subtraction of (59) from (60), we see we can write (61) in vector form as $\boldsymbol{y} = \boldsymbol{y}^H - (\rho - \rho^H)\boldsymbol{\mu}^\infty$. Taking $\boldsymbol{y} = \boldsymbol{y}^0 = \left(y_1^0, y_2^0, y_3^0\right)$ in (61), where $\boldsymbol{y}^0$ is a point on the ground, shows that $\boldsymbol{\mu}^\infty = \epsilon_\infty(\widehat{\boldsymbol{y}^H - \boldsymbol{y}^0})$.

The same arguments apply to the second line of (57), except that now the third components of $\boldsymbol{\eta}_\downarrow^+$ and $\boldsymbol{\eta}_\downarrow^\infty$ are negative. Thus $\boldsymbol{\eta}_\downarrow^+ = -(\widehat{\boldsymbol{\gamma}(s) - \boldsymbol{y}^H})$ and $\boldsymbol{\eta}_\downarrow^\infty = -\epsilon_\infty(\widehat{\boldsymbol{y}^H - \boldsymbol{y}^0})$. □

Proposition 3 implies that we can write the phase as

$$\begin{aligned}\phi(t,s,x,\omega,\tilde{\boldsymbol{\mu}}_T,\tilde{\boldsymbol{\mu}}_T) &= -\omega\big(t - \big[\boldsymbol{\mu}^+\cdot(\boldsymbol{\gamma}(s)-\boldsymbol{x}^H) + \boldsymbol{\mu}^\infty\cdot(\boldsymbol{x}^H-\boldsymbol{x}) \\ &\qquad + \boldsymbol{\eta}^+_\downarrow\cdot(\boldsymbol{x}^H-\boldsymbol{\gamma}(s)) + \boldsymbol{\eta}^\infty_\downarrow\cdot(\boldsymbol{x}-\boldsymbol{x}^H)\big]\big/c_0\big) \\ &= -\omega(t - 2(|\boldsymbol{\gamma}(s)-\boldsymbol{x}^H| + \epsilon_\infty|\boldsymbol{x}^H-\boldsymbol{x}|)/c_0). \end{aligned} \tag{62}$$

From (62), the interpretation of the phase in terms of travel time is clear.

Proposition 4. *Under assumption 4, equations (55) (and (56)) can be solved for $\boldsymbol{\mu}_T$ (and $\boldsymbol{\eta}_T$) in terms of $\boldsymbol{\gamma}(s)$ and $\boldsymbol{x}$.*

Proof. First we note that if we write $\boldsymbol{\mu}_T$ in polar coordinates, solving (55) for $\boldsymbol{\mu}$ really requires only solving for the single variable $r = \left(\mu_1^2+\mu_2^2\right)^{1/2}$. This we see from writing the first line of (57) in the form

$$\gamma_j(s) - x_j = \mu_j\left(\frac{\gamma_3(s)-H}{\mu_3^+} + \frac{H-x_3^0}{\mu_\infty}\right), \tag{63}$$

for $j = 1, 2$ and dividing the $j = 2$ equation by the $j = 1$ equation. We find that

$$\tan\theta(s,\boldsymbol{x}) := \frac{\gamma_2(s)-x_1}{\gamma_1(s)-x_2} = \frac{\mu_2}{\mu_1}. \tag{64}$$

Thus knowledge of s and $\boldsymbol{x}$ determines θ. Formula (64) determines θ up to an additive factor of π; knowledge of the positions of $\boldsymbol{\gamma}(s)$ and $\boldsymbol{x}$ determine the correct quadrant for θ.

We write

$$\boldsymbol{\mu}_T = (r\cos\theta, r\sin\theta), \qquad \boldsymbol{\gamma}_T(s) - \boldsymbol{x}_T = (R\cos\theta, R\sin\theta). \tag{65}$$

With this notation, we have $\mu_3^+ = (1-r^2)^{1/2}$ and $\mu_\infty = (\epsilon_\infty - r^2)^{1/2}$, and each equation of (63) can be written as

$$\frac{R}{r} = \frac{\gamma_3(s)-H}{\sqrt{1-r^2}} + \frac{H-x_3^0}{\sqrt{\epsilon_\infty - r^2}}. \tag{66}$$

We rewrite this equation as

$$0 = f(s,\boldsymbol{x},r) := \frac{r}{\sqrt{1-r^2}}(\gamma_3(s)-H) + \frac{r}{\sqrt{\epsilon_\infty-r^2}}\left(H-x_3^0\right) - R(s,\boldsymbol{x}), \tag{67}$$

where $R(s,\boldsymbol{x}) = |\boldsymbol{\gamma}_T(s) - \boldsymbol{x}_T|$. The implicit function theorem guarantees that we can solve (67) for r in terms of s, x_1 and x_2 whenever $\partial f/\partial r \neq 0$. We calculate

$$\frac{\partial f}{\partial r} = \frac{\gamma_3(s)-H}{[1-r^2]^{3/2}} + \epsilon_\infty\frac{H-x_3^0}{[\epsilon_\infty-r^2]^{3/2}} = \frac{\gamma_3(s)-H}{\left(\mu_3^+\right)^3} + \epsilon_\infty\frac{H-x_3^0}{\mu_\infty^3} \neq 0. \tag{68}$$

The argument for (56) is similar. □

Proposition 4 says that the takeoff direction $-\boldsymbol{\mu}^+ = \boldsymbol{\eta}^+_\downarrow$ of the refracting ray is determined by its initial position $\boldsymbol{\gamma}(s)$ and its final position $\boldsymbol{x}$. (This is intuitively clear from Snell's law.) We denote by $\boldsymbol{\mu}_T(s,\boldsymbol{x})$ (and correspondingly $r(s,\boldsymbol{x})$ and $\theta(s,\boldsymbol{x})$) the solution of (55) determined by proposition 4.

We note that an explicit formula for $\boldsymbol{\mu}_T$ in terms of s and $\boldsymbol{x}$ could be obtained by converting Snell's law (which is encoded in the definitions of $\boldsymbol{\mu}^+_\downarrow$ and $\boldsymbol{\mu}^\infty$) into a fourth-order polynomial for the coordinates of $\boldsymbol{x}^H$.

Although an explicit formula for $\boldsymbol{\mu}_T$ in terms of s is complicated, a formula for $\partial\boldsymbol{\mu}_T/\partial s$ (needed in the next section) can be obtained by implicit differentiation.

Corollary 2.

$$\begin{aligned}
\frac{\partial \mu_1}{\partial s} &= -\cos\theta \frac{\dfrac{r}{\mu_3^+}\dot{\gamma}_3(s) - (\dot{\gamma}_1\cos\theta + \dot{\gamma}_2\sin\theta)}{\dfrac{\gamma_3(s) - H}{\left(\mu_3^+\right)^3} + \epsilon_\infty \dfrac{H - x_3^0}{\mu_\infty^3}} + \frac{r}{R}\sin\theta(\dot{\gamma}_1\sin\theta - \dot{\gamma}_2\cos\theta), \\
\frac{\partial \mu_2}{\partial s} &= -\sin\theta \frac{\dfrac{r}{\mu_3^+}\dot{\gamma}_3(s) - (\dot{\gamma}_1\cos\theta + \dot{\gamma}_2\sin\theta)}{\dfrac{\gamma_3(s) - H}{\left(\mu_3^+\right)^3} + \epsilon_\infty \dfrac{H - x_3^0}{\mu_\infty^3}} - \frac{r}{R}\cos\theta(\dot{\gamma}_1\sin\theta - \dot{\gamma}_2\cos\theta).
\end{aligned} \tag{69}$$

Here $\theta = \theta(s, \boldsymbol{x})$ *and* $r = r(s, \boldsymbol{x})$.

Proof. From the chain rule applied to (65), we have

$$\begin{aligned}
\frac{\partial \mu_1}{\partial s} &= \frac{\partial \mu_1}{\partial r}\frac{\partial r}{\partial s} + \frac{\partial \mu_1}{\partial \theta}\frac{\partial \theta}{\partial s} = \cos\theta \frac{-\partial f/\partial s}{\partial f/\partial r} + r\sin\theta\frac{1}{R}(\dot{\gamma}_1\sin\theta - \dot{\gamma}_2\cos\theta), \\
\frac{\partial \mu_2}{\partial s} &= \frac{\partial \mu_2}{\partial r}\frac{\partial r}{\partial s} + \frac{\partial \mu_2}{\partial \theta}\frac{\partial \theta}{\partial s} = \sin\theta \frac{-\partial f/\partial s}{\partial f/\partial r} - r\cos\theta\frac{1}{R}(\dot{\gamma}_1\sin\theta - \dot{\gamma}_2\cos\theta),
\end{aligned} \tag{70}$$

where in the second equality we have used the implicit function theorem applied to (67) to obtain $\partial r/\partial s$ and applied to (65) as follows to obtain $\partial\theta/\partial s$. In particular, we consider the second equation of (65) to be two scalar equations that determine R and θ as functions of s (with $\boldsymbol{x}$ fixed). Implicit differentiation gives us

$$\dot{\gamma}_T = \begin{pmatrix}\cos\theta \\ \sin\theta\end{pmatrix}\frac{\partial R}{\partial s} + R\begin{pmatrix}-\sin\theta \\ \cos\theta\end{pmatrix}\frac{\partial\theta}{\partial s}; \tag{71}$$

solving for $\partial R/\partial s$ and $\partial\theta/\partial s$ gives us

$$\begin{aligned}
\frac{\partial R}{\partial s} &= \dot{\gamma}_1\cos\theta + \dot{\gamma}_2\sin\theta, \\
\frac{\partial \theta}{\partial s} &= \frac{-1}{R}(\dot{\gamma}_1\sin\theta - \dot{\gamma}_2\cos\theta).
\end{aligned} \tag{72}$$

We note that R cannot be zero by assumption 2. Differentiating (67), we have

$$\frac{\partial f}{\partial s} = \frac{r}{\mu_3^+}\dot{\gamma}_3(s) - \frac{\partial R}{\partial s} = \frac{r}{\mu_3^+}\dot{\gamma}_3(s) - (\dot{\gamma}_1\cos\theta + \dot{\gamma}_2\sin\theta). \tag{73}$$

Combining (70), (73) and (68) gives the result. □

3.3.2. Stationary-phase analysis of F. If we carry out a stationary-phase reduction of (47) in the variables $\tilde{\boldsymbol{\mu}}_T$ and $\tilde{\boldsymbol{\eta}}_T$, we find

$$\begin{aligned}
FV(s,t) = -\left(\frac{2\pi}{\omega}\right)^2 \int & \mathrm{e}^{\mathrm{i}\phi(t,s,\boldsymbol{x},\omega,\tilde{\boldsymbol{\mu}}_T,-\tilde{\boldsymbol{\mu}}_T)} A(t,s,\boldsymbol{x},\omega,\tilde{\boldsymbol{\mu}}_T,-\tilde{\boldsymbol{\mu}}_T) \\
& \times V(\boldsymbol{x}_T)\left|\det D_\mu^2\phi\right|^{-1}(s,\boldsymbol{x},\tilde{\boldsymbol{\mu}}_T)\,\mathrm{d}\omega\,\mathrm{d}^2\boldsymbol{x}_T + E_1(s,t),
\end{aligned} \tag{74}$$

where $\tilde{\boldsymbol{\mu}}_T$ is shorthand for $\tilde{\boldsymbol{\mu}}_T(s,\boldsymbol{x})$, and where the determinant of the Hessian of ϕ is given by

$$|\det D^2\phi|(s,\boldsymbol{x},\tilde{\boldsymbol{\mu}}_T) = \left|\det D_\mu^2\phi(s,\boldsymbol{x},\tilde{\boldsymbol{\mu}}_T)\right|^2, \tag{75}$$

with

$$\left|D_\mu^2\phi\right|(s,\boldsymbol{x},\tilde{\boldsymbol{\mu}}_T) = \frac{1}{c_0^2}\left[\left(\frac{H-x_3^0}{\tilde{\mu}_\infty^3}((\tilde{\mu}_\infty)^3+|\tilde{\boldsymbol{\mu}}_T|^2/\omega^2)+\frac{(\gamma_3(s)-H)}{\left(\tilde{\mu}_3^+\right)^3}\left(\left(\tilde{\mu}_3^+\right)^3+|\tilde{\boldsymbol{\mu}}_T|^2/\omega^2\right)\right)\right.$$
$$\left.\times\left(\frac{H-x_3^0}{\tilde{\mu}_\infty}+\frac{(\gamma_3(s)-H)}{\tilde{\mu}_3^+}\right)\right], \tag{76}$$

and where E_1 denotes a function smoother than the other terms on the right-hand side. The details of the stationary-phase calculation are given in appendix B.

3.3.3. The canonical relation. The directional ('microlocal') information about how F maps singularities is given by the (twisted) *canonical relation* Λ', which is a subset of the set of points $((s,t;\sigma,\tau),(\boldsymbol{x};\boldsymbol{\xi}))$ in phase space with $\sigma=\partial_s\phi$, $\tau=\partial_t\phi$, and $\boldsymbol{\xi}=-\nabla_{\boldsymbol{x}_T}\phi$ such that $(s,t,\boldsymbol{x},\omega,\tilde{\boldsymbol{\mu}}_T,\tilde{\boldsymbol{\eta}}_T)$ is in the critical set (54)–(56). Differentiating (48) and then using the fact that $\boldsymbol{\mu}_T=-\boldsymbol{\eta}_T$ on the critical set, we find

$$\begin{aligned}\Lambda' = \Big\{&((s,t;\sigma,\tau),(\boldsymbol{x};\boldsymbol{\xi}))\in\text{essential support of } A:\\ &t=2(|\gamma(s)-\boldsymbol{x}^H|+\epsilon_\infty|\boldsymbol{x}^H-\boldsymbol{x}|)/c_0\\ &\sigma=\partial_s\phi=\frac{1}{c_0}\left[\left(\tilde{\boldsymbol{\mu}}_T,\omega\tilde{\mu}_3^+\right)+\left(-\tilde{\boldsymbol{\eta}}_T,\omega\tilde{\eta}_3^+\right)\right]\cdot\dot{\gamma}(s)=2k\boldsymbol{\mu}^+\cdot\dot{\gamma}(s)\\ &\tau=\partial_t\phi=-\omega\\ &\boldsymbol{\xi}=-\nabla_{\boldsymbol{x}_T}\phi=\frac{\tilde{\boldsymbol{\mu}}_T-\tilde{\boldsymbol{\eta}}_T}{c_0}=2k\boldsymbol{\mu}_T\Big\}.\end{aligned} \tag{77}$$

Here the essential support of A denotes the subset of points on the critical set for which A does not correspond to an (infinitely) smoothing operator (i.e. A is not in the symbol class $S^{-\infty}=\cap_m S^m$). In other words, for the purpose of studying how F maps singularities, points in the complement of the essential support of A can be neglected. In our case, we have removed troublesome points with our taper function ψ; points for which ψ is zero are clearly not in the essential support of A and thus are not in Λ'.

4. Image formation

To form an image (i.e., an approximation to V), we would like to apply to the data an operator Q such that $QF=I$. Microlocal analysis shows us how to construct a *relative parametrix* Q for F so that $QF=I+$ (relatively smoothing operator), where by a relatively smoothing operator we mean one that improves the smoothness. The operator Q is constructed as an FIO

$$(Qd)(\boldsymbol{z})=\int \mathrm{e}^{-\mathrm{i}\phi(t,s,\boldsymbol{z},\omega,\tilde{\boldsymbol{\mu}}_T,\tilde{\boldsymbol{\eta}}_T)}B(t,s,\boldsymbol{z},\omega,\tilde{\boldsymbol{\mu}}_T,\tilde{\boldsymbol{\eta}}_T)d(s,t)\,\mathrm{d}\omega\,\mathrm{d}^2\tilde{\boldsymbol{\eta}}_T\,\mathrm{d}^2\tilde{\boldsymbol{\mu}}_T\,\mathrm{d}s\,\mathrm{d}t, \tag{78}$$

whose phase is the negative of the phase of F. We note that the phase of (78) is the same as that of the adjoint F^*. At this point the amplitude B is not known; it will be determined below.

4.1. Composition of Q and F

The composition of two FIOs does not always make sense. Here we rely on the following theorem [39], which gives a criterion involving the projection P from points $((s,t;\sigma,\tau),(\boldsymbol{x},\boldsymbol{\xi}))\in\Lambda'$ to the 'output variables' $(s,t;\sigma,\tau)$:

Theorem 1. *If the canonical relation Λ' of F is such that the projection P is an injective immersion (i.e., is one-to-one and its derivative DP is also one-to-one), then F^* (or Q) can be composed with F, and the composite operator F^*F (resp. QF) is again an FIO.*

The conditions of this theorem are not satisfied unless we make an additional assumption about the antenna beam patterns.

Assumption 8. The antenna beam pattern $\tilde{J}_s$ or $\tilde{J}_r$ directs radiation to one side of the flight path, so that the product $\tilde{J}_s(\omega, s, \tilde{\boldsymbol{\mu}}/\omega)\tilde{J}_r(\omega, s, \tilde{\boldsymbol{\eta}}/\omega)$ is negligible when $\left[\boldsymbol{\mu}^+_\downarrow(s, \boldsymbol{x}) \times \dot{\boldsymbol{\gamma}}(s)\right]_3 \leqslant 0$ and $\left[\boldsymbol{\eta}^+_\downarrow(s, \boldsymbol{x}) \times \dot{\boldsymbol{\gamma}}(s)\right]_3 \leqslant 0$ (the reverse inequalities hold if the radiation is directed to the other side).

In other words, we assume that the essential support of A contains only points for which $[(\boldsymbol{\gamma}(s) - \boldsymbol{x}^H) \times \dot{\boldsymbol{\gamma}}(s)]_3$ is strictly positive (or strictly negative, depending on how the antenna is mounted). If this assumption is not satisfied, QF is not an FIO, and this implies that the image QF contains certain artefacts [38].

Proposition 5. *Under assumptions 1–8, the canonical relation of F satisfies the hypotheses of theorem 1.*

The proof of this proposition is contained in appendix C.

4.2. Determination of Q

To determine the amplitude B that will make QF approximately the identity operator, we apply the operator Q to the data $d = FV$:

$$\begin{aligned}(QFV)(\boldsymbol{z}) = \int & \mathrm{e}^{-\mathrm{i}\phi(t,s,\boldsymbol{z},\omega,\tilde{\boldsymbol{\mu}}_T,\tilde{\boldsymbol{\eta}}_T)} B(t, s, \boldsymbol{z}, \omega, \tilde{\boldsymbol{\mu}}_T, \tilde{\boldsymbol{\eta}}_T) \\ & \times \int \mathrm{e}^{\mathrm{i}\phi(t,s,\boldsymbol{x},\omega',\tilde{\boldsymbol{\mu}}'_T,\tilde{\boldsymbol{\eta}}'_T)} A(t, s, \boldsymbol{x}, \omega', \tilde{\boldsymbol{\mu}}'_T, \tilde{\boldsymbol{\eta}}'_T) V(x_T) \\ & \times \mathrm{d}^2\tilde{\mu}'_T\, \mathrm{d}^2\tilde{\boldsymbol{\eta}}'_T\, \mathrm{d}\omega'\, \mathrm{d}^2 x_T\, \mathrm{d}\omega\, \mathrm{d}^2\tilde{\boldsymbol{\eta}}_T\, \mathrm{d}^2\tilde{\boldsymbol{\mu}}_T\, \mathrm{d}s\, \mathrm{d}t, \end{aligned} \tag{79}$$

where $\boldsymbol{z} = (\boldsymbol{z}_T, 0)$. We then carry out the following calculations.

4.2.1. Simplification of QF by stationary phase. In (79) we apply the method of stationary phase in the pair of variables ω', t. For this calculation, we write the phase ϕ as $\phi(t, s, \boldsymbol{x}, \omega, \tilde{\boldsymbol{\mu}}_T, \tilde{\boldsymbol{\eta}}_T) = -\omega t + \varphi(s, \boldsymbol{x}, \omega, \tilde{\boldsymbol{\mu}}_T, \tilde{\boldsymbol{\eta}}_T)$, where

$$\begin{aligned}\varphi(s, \boldsymbol{x}, \omega, \tilde{\boldsymbol{\mu}}_T, \tilde{\boldsymbol{\eta}}_T) &= k\left(\frac{\tilde{\boldsymbol{\mu}}_T}{\omega} \cdot (\boldsymbol{\gamma}_T(s) - \boldsymbol{x}_T) + \tilde{\mu}_\infty(H - x_3) + \tilde{\mu}^+_3(\gamma_3(s) - H)\right. \\ &\quad \left. + \frac{\tilde{\boldsymbol{\eta}}_T}{\omega} \cdot (\boldsymbol{x}_T - \boldsymbol{\gamma}_T(s)) + \tilde{\eta}_\infty(H - x_3) + \tilde{\eta}^+_3(\gamma_3(s) - H)\right) \\ &= k\left[\boldsymbol{\mu}^+ \cdot (\boldsymbol{\gamma}(s) - \boldsymbol{x}^H) + \boldsymbol{\mu}^\infty \cdot (\boldsymbol{x}^H - \boldsymbol{x}) + \boldsymbol{\eta}^+_\downarrow \cdot (\boldsymbol{x}^H - \boldsymbol{\gamma}(s)) + \boldsymbol{\eta}^\infty_\downarrow \cdot (\boldsymbol{x} - \boldsymbol{x}^H)\right], \end{aligned} \tag{80}$$

where $\boldsymbol{\mu}^+ = \left(\tilde{\boldsymbol{\mu}}_T/\omega, \tilde{\mu}^+_3\right) = (\boldsymbol{\mu}_T, \mu_3)$, etc. A careful calculation requires that we use the homogeneity of φ and a number of changes of variables to bring out ω as the large parameter in order to apply the stationary-phase theorem; however, the end result is the same

as if we had simply used $\int \exp[\mathrm{i}t(\omega-\omega')]\,\mathrm{d}t = 2\pi\delta(\omega-\omega')$ and evaluated the result at $t = t_\varphi(s, \boldsymbol{x}, \omega, \tilde{\boldsymbol{\mu}}'_T, \tilde{\boldsymbol{\eta}}'_T) = \varphi(s, \boldsymbol{x}, 1, \tilde{\boldsymbol{\mu}}'_T/\omega, \tilde{\boldsymbol{\eta}}'_T/\omega)$. Thus we obtain

$$
\begin{aligned}
(QFV)(\boldsymbol{z}_T) = 2\pi \int & \mathrm{e}^{-\mathrm{i}\varphi(s,\boldsymbol{z},\omega,\tilde{\boldsymbol{\mu}}_T,\tilde{\boldsymbol{\eta}}_T)} B(t_\varphi, s, \boldsymbol{z}, \omega, \tilde{\boldsymbol{\mu}}_T, \tilde{\boldsymbol{\eta}}_T) \\
& \times \int \mathrm{e}^{\mathrm{i}\varphi(s,\boldsymbol{x},\omega,\tilde{\boldsymbol{\mu}}'_T,\tilde{\boldsymbol{\eta}}'_T)} A(t_\varphi, s, \boldsymbol{x}, \omega, \tilde{\boldsymbol{\mu}}'_T, \tilde{\boldsymbol{\eta}}'_T) V(\boldsymbol{x}_T) \\
& \times \mathrm{d}^2\tilde{\boldsymbol{\mu}}'_T\, \mathrm{d}^2\tilde{\boldsymbol{\eta}}'_T\, \mathrm{d}^2\boldsymbol{x}_T\, \mathrm{d}\omega\, \mathrm{d}^2\tilde{\boldsymbol{\eta}}_T\, \mathrm{d}^2\tilde{\boldsymbol{\mu}}_T\, \mathrm{d}s + E_2(\boldsymbol{z}_T),
\end{aligned} \tag{81}
$$

where E_2 is one degree smoother than the first term.

Next we carry out a stationary-phase reduction in the variables $\tilde{\boldsymbol{\mu}}_T$, $\tilde{\boldsymbol{\eta}}_T$, $\tilde{\boldsymbol{\mu}}'_T$, and $\tilde{\boldsymbol{\eta}}'_T$. These calculations are the same as done in the stationary-phase analysis (74) of F. This process results in

$$
\begin{aligned}
(QFV)(\boldsymbol{z}) = \frac{(2\pi)^5}{\omega^4} \int & \mathrm{e}^{\mathrm{i}[\varphi(s,\boldsymbol{x},\omega,\tilde{\boldsymbol{\mu}}_T(s,\boldsymbol{x}),-\tilde{\boldsymbol{\mu}}_T(s,\boldsymbol{x}))-\varphi(s,\boldsymbol{z},\omega,\tilde{\boldsymbol{\mu}}_T(s,\boldsymbol{z}),-\tilde{\boldsymbol{\mu}}_T(s,\boldsymbol{z}))]} \\
& \times B(t_\varphi, s, \boldsymbol{z}, \omega, \tilde{\boldsymbol{\mu}}_T(s,\boldsymbol{z}), -\tilde{\boldsymbol{\mu}}_T(s,\boldsymbol{z})) \left|D^2_\mu\phi\right|^{-1}(s, \boldsymbol{z}, \tilde{\boldsymbol{\mu}}_T(s,\boldsymbol{z})) \\
& \times A(t_\varphi, s, \boldsymbol{x}, \omega, \tilde{\boldsymbol{\mu}}_T(s,\boldsymbol{x}), -\tilde{\boldsymbol{\mu}}_T(s,\boldsymbol{x})) \left|D^2_\mu\phi\right|^{-1}(s, \boldsymbol{x}, \tilde{\boldsymbol{\mu}}_T(s,\boldsymbol{x})) \\
& \times V(\boldsymbol{x}_T)\, \mathrm{d}^2\boldsymbol{x}_T\, \mathrm{d}\omega\, \mathrm{d}s + E_3(\boldsymbol{z}),
\end{aligned} \tag{82}
$$

where again E_3 denotes a smoother term.

4.2.2. Change of variables. Next we expand the phase in a Taylor series about the point $z_T = x_T$:

$$
\begin{aligned}
\varphi(s, \boldsymbol{x}, \omega, \tilde{\boldsymbol{\mu}}_T(s,\boldsymbol{x}), -\tilde{\boldsymbol{\mu}}_T(s,\boldsymbol{x})) - \varphi(s, \boldsymbol{z}, \omega, \tilde{\boldsymbol{\mu}}_T(s,\boldsymbol{z}), -\tilde{\boldsymbol{\mu}}_T(s,\boldsymbol{z})) \\
= (\boldsymbol{z}-\boldsymbol{x})_T \cdot \Xi(\boldsymbol{z}, s, \boldsymbol{x}, \omega),
\end{aligned} \tag{83}
$$

where

$$
\Xi(\boldsymbol{z}, s, \boldsymbol{x}, \omega) = \int_0^1 \nabla_{\boldsymbol{y}_T}\varphi(s, \boldsymbol{y}, \omega, \tilde{\boldsymbol{\mu}}_T(s,\boldsymbol{y}), -\tilde{\boldsymbol{\mu}}_T(s,\boldsymbol{y}))\Big|_{\boldsymbol{y}=\boldsymbol{x}+\lambda(\boldsymbol{z}-\boldsymbol{x})} \mathrm{d}\lambda. \tag{84}
$$

In (82) we now make the change of variables (justified below)

$$
(s, \omega) \to \boldsymbol{\xi} = \Xi(\boldsymbol{z}, s, \boldsymbol{x}, \omega), \tag{85}
$$

which transforms (82) into

$$
\begin{aligned}
(QFV)(\boldsymbol{z}) = \int & \mathrm{e}^{\mathrm{i}(\boldsymbol{z}-\boldsymbol{x})_T\cdot\boldsymbol{\xi}} B(t_\varphi, s, \boldsymbol{z}, \omega, \tilde{\boldsymbol{\mu}}_T(s,\boldsymbol{z}), -\tilde{\boldsymbol{\mu}}_T(s,\boldsymbol{z})) \\
& \times A(t_\varphi, s, \boldsymbol{x}, \omega, \tilde{\boldsymbol{\mu}}_T(s,\boldsymbol{x}), -\tilde{\boldsymbol{\mu}}_T(s,\boldsymbol{x})) \\
& \times \left|D^2_\mu\phi\right|^{-1}(s, \boldsymbol{z}, \tilde{\boldsymbol{\mu}}_T(s,\boldsymbol{z})) \left|D^2_\mu\phi\right|^{-1}(s, \boldsymbol{x}, \tilde{\boldsymbol{\mu}}_T(s,\boldsymbol{x})) \\
& \times \left|\frac{\partial(s,\omega)}{\partial\boldsymbol{\xi}}\right|(\boldsymbol{z}, s, \boldsymbol{x}, \omega) V(\boldsymbol{x}_T)\, \mathrm{d}^2\boldsymbol{x}_T\, \mathrm{d}\boldsymbol{\xi} + E_4(\boldsymbol{z}),
\end{aligned} \tag{86}
$$

where in (86), $s = s(\boldsymbol{\xi})$, $\omega = \omega(\boldsymbol{\xi})$ and $t_\varphi = t_\varphi(s, \boldsymbol{x}, \omega, \tilde{\boldsymbol{\mu}}'_T, -\tilde{\boldsymbol{\mu}}'_T)$. We see that the phase of (86) is the same as that of a delta function $\delta(\boldsymbol{z}-\boldsymbol{x}) \propto \int \exp[\mathrm{i}(\boldsymbol{z}-\boldsymbol{x})_T \cdot \boldsymbol{\xi}]\,\mathrm{d}\boldsymbol{\xi}$, which, together with the estimates of proposition 2, means that the operator QF is a pseudodifferential operator. Pseudodifferential operators have the *pseudolocal* property [44], i.e., they do not move singularities or change their orientation. This means that the imaging operator Q correctly reconstructs the edges and interfaces that are visible in the original scene.

Mathematically, QF's preservation of visible singularities is due to the fact that the leading order contribution to (86) comes from the point $\boldsymbol{z}_T = \boldsymbol{x}_T$.

Calculation of the Jacobian determinant. To calculate the Jacobian determinant when $\boldsymbol{z} = \boldsymbol{x}$, we note that since

$$\varphi(s, \boldsymbol{x}, \omega, \tilde{\boldsymbol{\mu}}_T(s, x), -\tilde{\boldsymbol{\mu}}_T(s, x)) = 2k(|\boldsymbol{\gamma}(s) - \boldsymbol{x}^H| + \epsilon_\infty |\boldsymbol{x}^H - \boldsymbol{x}|), \tag{87}$$

the $\nabla\varphi$ appearing in (84) is

$$\begin{aligned}\nabla_{x_T}\varphi(s, \boldsymbol{x}, \omega, \tilde{\boldsymbol{\mu}}_T(s, \boldsymbol{x}), -\tilde{\boldsymbol{\mu}}_T(s, \boldsymbol{x}))\\ &= 2k(-(\widehat{\gamma(s) - \boldsymbol{x}^H}) \cdot D_T\boldsymbol{x}^H + \epsilon_\infty(\widehat{\boldsymbol{x}^H - \boldsymbol{x}}) \cdot (D_T\boldsymbol{x}^H - \boldsymbol{I}_T))\\ &= 2k[\boldsymbol{\mu}^+ \cdot D_T\boldsymbol{x}^H - \boldsymbol{\mu}^\infty \cdot (D_T\boldsymbol{x}^H - \boldsymbol{I}_T)],\end{aligned} \tag{88}$$

where

$$\boldsymbol{I}_T = \begin{pmatrix} 1 & 0 \\ 0 & 1 \\ 0 & 0 \end{pmatrix}, \tag{89}$$

and $D_T\boldsymbol{x}^H$ is a 3×2 matrix composed of the column vectors

$$D_T\boldsymbol{x}^H = \left(\frac{\partial \boldsymbol{x}^H}{\partial x_1}, \frac{\partial \boldsymbol{x}^H}{\partial x_2}\right). \tag{90}$$

We note that the bottom row of the matrices $D_T\boldsymbol{x}^H$ and $\boldsymbol{I}_T$ is zero; since $\boldsymbol{\mu}_T^+ = \boldsymbol{\mu}_T^\infty$, this implies that (88) can be written as

$$\nabla\varphi(s, \boldsymbol{x}, \omega, \tilde{\boldsymbol{\mu}}_T(s, \boldsymbol{x}), -\tilde{\boldsymbol{\mu}}_T(s, \boldsymbol{x})) = 2k\boldsymbol{\mu}_T \cdot (D_T\boldsymbol{x}^H - D_T\boldsymbol{x}^H + \boldsymbol{I}_T) = 2k\boldsymbol{\mu}_T. \tag{91}$$

Thus at $\boldsymbol{x} = \boldsymbol{z}$, we have

$$\boldsymbol{\xi} = 2k\boldsymbol{\mu}_T. \tag{92}$$

This implies that the Jacobian determinant is

$$\left|\frac{\partial \boldsymbol{\xi}}{\partial(s, \omega)}\right| = \begin{vmatrix} 2k\frac{\partial \mu_1}{\partial s} & 2k\frac{\partial \mu_2}{\partial s} \\ \frac{2\mu_1}{c} & \frac{2\mu_2}{c} \end{vmatrix} = \frac{4k}{c}\left(\mu_2\frac{\partial \mu_1}{\partial s} - \mu_1\frac{\partial \mu_2}{\partial s}\right). \tag{93}$$

From corollary 2 and (65), we find

$$\begin{aligned}\left|\frac{\partial \boldsymbol{\xi}}{\partial(s, \omega)}\right| = \frac{4k}{c}\Bigg[r\sin\theta\Bigg(&-\cos\theta\frac{\frac{r}{\mu_3^+}\dot{\gamma}_3(s) - (\dot{\gamma}_1\cos\theta + \dot{\gamma}_2\sin\theta)}{\frac{\gamma_3(s)-H}{(\mu_3^+)^3} + \epsilon_\infty\frac{H-x_3^0}{\mu_\infty^3}}\\ &- \frac{r}{R}\sin\theta(\dot{\gamma}_2\cos\theta - \dot{\gamma}_1\sin\theta)\Bigg)\\ &- r\cos\theta\Bigg(-\sin\theta\frac{\frac{r}{\mu_3^+}\dot{\gamma}_3(s) - (\dot{\gamma}_1\cos\theta + \dot{\gamma}_2\sin\theta)}{\frac{\gamma_3(s)-H}{(\mu_3^+)^3} + \epsilon_\infty\frac{H-x_3^0}{\mu_\infty^3}}\\ &+ \frac{r}{R}\cos\theta(\dot{\gamma}_2\cos\theta - \dot{\gamma}_1\sin\theta)\Bigg)\Bigg]\\ = -\frac{4k}{c}\left[\frac{r^2}{R}(\dot{\gamma}_2\cos\theta - \dot{\gamma}_1\sin\theta)\right] &= \frac{4k}{c}\frac{r}{R}\dot{\boldsymbol{\gamma}}_T(s) \cdot \boldsymbol{\mu}_T^\perp,\end{aligned} \tag{94}$$

where $\boldsymbol{\mu}_T^\perp = r(\sin\theta, -\cos\theta)$.

Explicit calculation of this expression for use in the backprojection operator requires knowledge of $\boldsymbol{\mu}_T$ in terms of s and $\boldsymbol{x}$.

We see from (94) that the change of variables (85) can be made everywhere except along the tangent to the flight path. This region is already excluded by assumption 8.

4.2.3. The imaging operator. We see from (87) that we can use a somewhat simplified form of Q, namely

$$(\tilde{Q}d)(\boldsymbol{z}) = \int \mathrm{e}^{-\mathrm{i}\omega(t-2[|\gamma(s)-\boldsymbol{z}^H|+\epsilon_\infty|\boldsymbol{z}^H-\boldsymbol{z}|]/c_0)}\,\tilde{B}(\boldsymbol{z}, s, \omega)d(s, t)\,\mathrm{d}\omega\,\mathrm{d}s\,\mathrm{d}t, \qquad (95)$$

where

$$\tilde{B}(\boldsymbol{z}, s, \omega) = \frac{-\left|\frac{\partial\boldsymbol{\xi}}{\partial(s,\omega)}\right|(\boldsymbol{z}, s, \boldsymbol{z}, \omega)\left|D^2_\mu\phi\right|^2(s, \boldsymbol{z}, (\widehat{\gamma(s)-\boldsymbol{z}^H})_T)\chi(\boldsymbol{z}, s, \omega)}{A(\varphi(s, \boldsymbol{z}, 1, \widehat{\gamma(s)-\boldsymbol{z}^H}, \widehat{\boldsymbol{z}^H-\gamma(s)}), s, \boldsymbol{z}, \omega, \widehat{\gamma(s)-\boldsymbol{z}^H}, \widehat{\boldsymbol{z}^H-\gamma(s)})}, \qquad (96)$$

where $\chi(\boldsymbol{z}, s, \omega)$ is a smooth cutoff function that prevents division by zero in (96).

Stationary phase analysis of $\tilde{Q}F$ shows, as above, that $\tilde{Q}F = I+$ (smoothing operator of degree 1); this means that the operator $\tilde{Q}$, when applied to the data, produces a bandlimited version of an image in which the singularities of V have the correct positions and strengths. In particular, the leading order behaviour of the kernel of QF is the approximate delta function $\int \exp[\mathrm{i}(\boldsymbol{z}-\boldsymbol{x})_T \cdot \boldsymbol{\xi}]\,\mathrm{d}\boldsymbol{\xi}$.

The degree to which the point spread function (kernel of QF) approximates a delta function (i.e. the resolution of the system) is determined by the region of $\boldsymbol{\xi}$ integration. This region is determined, via relation (92), by the bandwidth, antenna beam pattern and geometry of the data collection curve. The resolution is actually slightly better than if the dispersive layer were absent; this is because when the ray path from $\gamma(s)$ to $\boldsymbol{x}$ is bent downwards by the refracting medium (as in figure 2), the horizontal components of μ_T are slightly larger than they would be if the ray path were straight.

The image of the singularities of V could be enhanced by using, instead of $\tilde{Q}$, an operator Q_1, which is the same as $\tilde{Q}$ except that $\tilde{B}$ is replaced by $B_1 = |\boldsymbol{\xi}|\tilde{B} = 2k|\boldsymbol{\mu}_T|\tilde{B}$. The leading order behaviour of Q_1F is then $\int |\boldsymbol{\xi}| \exp[\mathrm{i}(\boldsymbol{z}-\boldsymbol{x})_T \cdot \boldsymbol{\xi}]\,\mathrm{d}\boldsymbol{\xi}$, a pseudodifferential operator of order 1. The resulting image would be an approximation to $|\nabla V|$, in which jump discontinuities of V would appear as (bandlimited) delta functions.

It is theoretically possible to obtain an approximation $Q^\#$ to F^{-1} that, rather than being good only to first order as are Q and $\tilde{Q}$, is good to all orders of smoothness. This could be done by using the full stationary-phase expansion [19] in the places where we have used simply the first-order stationary-phase approximation. The amplitude of the resulting operator $Q^\#$ would be more complicated, but its leading order term would be given by (96).

For dispersive materials, $\epsilon_r(\omega)$ is always complex, which implies that such materials are dissipative to some degree. This, in turn, implies that for some problems the amplitude A may be quite small, and consequently the inversion of (96) may tend to amplify noise. Investigation of this issue is left for the future.

5. Conclusions

We have shown an image formation operator (95) that can be used for synthetic-aperture imaging through a homogeneous dispersive layer. We see from the phase of (95) that it is the *refraction* through the layer that must be accounted for in order to obtain a focused image. The dispersion can be corrected for by adjusting the amplitude B of the backprojection operator (95). This amplitude, however, does not affect the positioning of the edges in the image.

The refraction through the layer is determined by the high-frequency permittivity ϵ_∞. We leave for the future the following questions: (a) Can the high-frequency quantity ϵ_∞ be determined [30] from bandlimited data? (b) If ϵ_∞ is estimated incorrectly, what effect does this have on the image? (c) What is the best way to implement the algorithm numerically? and (d) How does the algorithm behave in the presence of noise?

Acknowledgments

We are grateful to Richard Albanese and Arje Nachman for drawing attention to the issue of dispersion in foliage-penetrating SAR. We thank Tom Roberts for helpful discussions regarding dispersive materials, and Sherwood Samn for reading the manuscript and catching a number of minor errors. MC's work was sponsored by the Air Force Office of Scientific Research[3] under agreement number F49620-03-1-0051. This work was also supported in part by the National Science Foundation through its Engineering Research Centers Program (award number EEC-9986821) and its Focused Research Groups in the Mathematical Sciences program.

Appendix A. Estimates for the amplitude $\tilde{a}$

We recall that $\tilde{a}$ is defined by

$$\tilde{a}(\omega, \tilde{\boldsymbol{\eta}}_T) = a(\omega, \tilde{\boldsymbol{\eta}}_T/\omega) = \psi(\omega, \tilde{\boldsymbol{\eta}}_T/\omega)\, \mathrm{e}^{\mathrm{i}k\tilde{\eta}_a(\omega,\tilde{\boldsymbol{\eta}}_T/\omega)(H-z_3^0)}. \tag{A.1}$$

We consider the various components of $\tilde{a}$ separately.

Lemma 1. *If assumption 6 holds, and in addition $|\boldsymbol{\eta}_T|^2$ is strictly bounded away from ϵ_∞, then η_a is smooth, and we have*

$$\left|\partial_{\eta_1}^{\beta_1}\partial_{\eta_2}^{\beta_2}\partial_{\omega}^{\beta_3}\eta_a(\omega, \boldsymbol{\eta}_T)\right| \leqslant C_\beta(1+\omega^2)^{-(1+\beta_3)/2}, \tag{A.2}$$

where β_1, β_2 and β_3 are non-negative integers. The constant C_β is zero if $\beta_1 > 2$ or $\beta_2 > 2$ or $\beta_1 + \beta_2 \geqslant 2$.

Proof. When $\boldsymbol{\beta} = 0$, we have

$$\begin{aligned}
\eta_a(\omega, \boldsymbol{\eta}_T) &= \eta_3^-(\omega, \boldsymbol{\eta}_T) - \eta_\infty^-(\boldsymbol{\eta}_T) \\
&= \sqrt{\epsilon_\infty + \epsilon_s(\omega) - |\boldsymbol{\eta}_T|^2} - \sqrt{\epsilon_\infty - |\boldsymbol{\eta}_T|^2} \\
&= \sqrt{\epsilon_\infty - |\boldsymbol{\eta}_T|^2}\left(\sqrt{1 + \frac{\epsilon_s(\omega)}{(\epsilon_\infty - |\boldsymbol{\eta}_T|^2)}} - 1\right) \\
&= \eta_\infty^-(\boldsymbol{\eta}_T)\left[\frac{1}{2}\frac{\epsilon_s(\omega)}{(\eta_\infty^-)^2} + O\left(\left|\frac{\epsilon_s(\omega)}{(\eta_\infty^-)^2}\right|^2\right)\right] \\
&= \frac{1}{2}\frac{\epsilon_s(\omega)}{\eta_\infty^-} + O\left(\frac{|\epsilon_s(\omega)|^2}{(\eta_\infty^-)^3}\right) \\
&= O((1+\omega^2)^{-1/2}),
\end{aligned} \tag{A.3}$$

[3] Consequently the US Government is authorized to reproduce and distribute reprints for Governmental purposes notwithstanding any copyright notation thereon. The views and conclusions contained herein are those of the authors and should not be interpreted as necessarily representing the official policies or endorsements, either expressed or implied, of the Air Force Research Laboratory or the US Government.

Table 1. The type of terms obtained from differentiation of $\sqrt{\zeta}$.

Derivative	Contains terms of the form
$\partial_\omega\sqrt{\zeta}$	$\zeta^{-1/2}(\partial_\omega\zeta)$
$\partial_{\eta_j}\sqrt{\zeta}$	$\zeta^{-1/2}\left(\partial_{\eta_j}\zeta\right)$
$\partial_{\eta_j}\partial_\omega\sqrt{\zeta}$	$\zeta^{-3/2}\left(\partial_{\eta_j}\zeta\right)(\partial_\omega\zeta)$, $\zeta^{-1/2}\partial_{\eta_j\omega}\zeta = 0$
$\partial^2_{\eta_j}\partial_\omega\sqrt{\zeta}$	$\zeta^{-5/2}\left(\partial_{\eta_j}\zeta\right)^2(\partial_\omega\zeta)$, $\zeta^{-3/2}\left(\partial^2_{\eta_j}\zeta\right)(\partial_\omega\zeta)$
$\partial^2_\omega\sqrt{\zeta}$	$\zeta^{-3/2}(\partial_\omega\zeta)^2$, $\zeta^{-1/2}\partial^2_\omega\zeta$
$\partial_{\eta_j}\partial^2_\omega\sqrt{\zeta}$	$\zeta^{-5/2}\left(\partial_{\eta_j}\zeta\right)(\partial_\omega\zeta)^2$, $\zeta^{-3/2}\left(\partial_{\eta_j}\zeta\right)\left(\partial^2_\omega\zeta\right)$

Table 2. The type of terms obtained from differentiation of $h = \omega\eta_a$.

Derivative	Contains terms of the form
$h = \omega\eta_a$	$\omega\eta_a$
$\partial_\omega h$	η_a, $\omega\partial_\omega\eta_a$
$\partial_{\eta_j}h$	$\omega\partial_{\eta_j}\eta_a$
$\partial^2_\omega h$	$(\partial_\omega\eta_a)$, $\omega\left(\partial^2_\omega\eta_a\right)$
$\partial_{\eta_j}\partial^n_\omega h$	$\partial_{\eta_j}\partial^{n-1}_\omega\eta_a$, $\omega\partial_{\eta_j}\partial^n_\omega\eta_a$

where in the fourth line we have used the expansion $\sqrt{1+x} = 1 + x/2 + O(x^2)$. We see that the estimate (A.2) is satisfied away from $|\boldsymbol{\eta}_T|^2 = \epsilon_\infty$ (where η^-_∞ is zero).

To check the derivatives, we use the temporary notation $\eta_a = \sqrt{\zeta} - \sqrt{\zeta_\infty}$, where $\zeta(\omega, \boldsymbol{\eta}) = \epsilon_\infty + \epsilon_s(\omega) - |\boldsymbol{\eta}_T|^2$ and $\zeta_\infty(\boldsymbol{\eta}) = \epsilon_\infty - |\boldsymbol{\eta}_T|^2$. We note that $\partial_\omega\zeta = \partial_\omega\epsilon_s$, $\partial_\omega\zeta_\infty = 0$, $\partial_{\eta_j}\zeta = \partial_{\eta_j}\zeta_\infty = 2\eta_j$, all mixed derivatives of ζ and ζ_∞ are zero and all η-derivatives of order higher than 2 are zero.

Derivatives of $\sqrt{\zeta}$ are shown in table 1.

Differentiations with respect to η_j are bounded because η_j is bounded. The reciprocal powers of ζ are bounded because the microlocal cutoff ψ causes $|\boldsymbol{\eta}_T|^2$ to be strictly bounded away from $\epsilon_\infty + \epsilon_s(\omega)$. We see that it is the order of the derivative with respect to ω that determines the large-ω behaviour.

The only nonzero derivatives of $\sqrt{\zeta_\infty}$ are those with respect to η_j; they follow the same pattern as the derivatives of $\sqrt{\zeta}$. □

We write $h = \omega\eta_a$.

Lemma 2. *If assumption 6 holds, and in addition $|\eta_T|^2$ is strictly bounded away from ϵ_∞, then h is smooth, and we have*

$$\left|\partial^{\beta_1}_{\eta_1}\partial^{\beta_2}_{\eta_2}\partial^{\beta_3}_\omega h(\omega, \boldsymbol{\eta}_T)\right| \leqslant C_\beta(1+\omega^2)^{-\beta_3/2}, \tag{A.4}$$

where β_1, β_2 and β_3 are non-negative integers. The constant C_β is zero if $\beta_1 > 2$ or $\beta_2 > 2$ or $\beta_1 + \beta_2 \geqslant 2$.

Proof. We show the derivatives of h in table 2. To the terms arising from $\partial^n_\omega h$, we apply lemma 1. □

Proof of proposition 1. We note that from the chain rule, we can write $\partial_\omega\tilde{a} = \partial_\omega a - (\boldsymbol{\eta}_T/\omega)\cdot\nabla_{\eta_T}a$. Since $\boldsymbol{\eta}_T$ is bounded, and further differentiations cannot introduce positive powers of ω, we see that (51) will be proved if we prove the version of (51) with the tildes removed.

Table 3. The type of terms obtained from differentiation of a.

Derivative	Contains terms of the form a multiplied by
$a = \psi\,\mathrm{e}^h$	1
$\partial_\omega a$	$\partial_\omega h$
$\partial_{\eta_j} a$	$\partial_{\eta_j} h$
$\partial_\omega^2 a$	$(\partial_\omega h)^2$, $\left(\partial_\omega^2 h\right)$
$\partial_{\eta_j}^2 a$	$\left(\partial_{\eta_j} h\right)^2$, $\left(\partial_{\eta_j}^2 h\right)$
$\partial_{\eta_j}\partial_\omega a$	$\left(\partial_{\eta_j} h\right)(\partial_\omega h)$, $\left(\partial_{\eta_j}\partial_\omega h\right)$,
$\partial_\omega^3 a$	$(\partial_\omega h)^3$, $(\partial_\omega h)\left(\partial_\omega^2 h\right)^2$, $\left(\partial_\omega^3 h\right)$
$\partial_{\eta_j}^2\partial_\omega a$	$\left(\partial_{\eta_j} h\right)^2(\partial_\omega h)$, $\left(\partial_{\eta_j}^2 h\right)(\partial_\omega h)$, $\left(\partial_{\eta_j} h\right)\left(\partial_{\eta_j}\partial\omega h\right)$, $\partial_{\eta_j}^2\partial_\omega h$
$\partial_{\eta_j}\partial_\omega^2 a$	$\left(\partial_{\eta_j}\partial_\omega h\right)(\partial_\omega h)$, $\left(\partial_{\eta_j} h\right)\left(\partial_\omega^2 h\right)$, $\left(\partial_{\eta_j} h\right)(\partial_\omega h)^2$, $\partial_{\eta_j}\partial_\omega^2 h$
$\partial_{\eta_j}^3 a$	$\left(\partial_{\eta_j} h\right)^3$, $\left(\partial_{\eta_j} h\right)\left(\partial_{\eta_j}^2 h\right)$, $\partial_{\eta_j}^3 h = 0$
$\partial_\omega^n a$	$(\partial_\omega h)^n, \ldots, \partial_\omega^n h$

We show derivatives of $a = \psi\,\mathrm{e}^h$ in table 3. Here we ignore terms involving derivatives of ψ because ψ is chosen so that all its derivatives decay more rapidly than any polynomial. We ignore also factors of $\left(H - z_3^0\right)/c$. Combining table 3 with the results of lemma 2 shows that the large-ω decay corresponds to the number of derivatives with respect to ω; this gives proposition 1. □

Appendix B. Stationary-phase calculations

The stationary-phase theorem states that [4, 19, 20]

Theorem 2. *If a is a smooth function of compact support on $\mathbf{R}^n$, and ϕ has only non-degenerate critical points, then as $\omega \to \infty$,*

$$\int \mathrm{e}^{\mathrm{i}\omega\phi(\boldsymbol{x})} a(\boldsymbol{x})\,\mathrm{d}^n\boldsymbol{x} = \sum_{\{\boldsymbol{x}^0 : D\phi(\boldsymbol{x}^0)=\mathbf{0}\}} \left(\frac{2\pi}{\omega}\right)^{n/2} a(\boldsymbol{x}^0)\frac{\mathrm{e}^{\mathrm{i}\omega\phi(\boldsymbol{x}^0)}\,\mathrm{e}^{\mathrm{i}(\pi/4)\mathrm{sgn}D^2\phi(\boldsymbol{x}^0)}}{\sqrt{|\det D^2\phi(\boldsymbol{x}^0)|}} + O(\omega^{-n/2-1}). \tag{B.1}$$

Here $D\phi$ denotes the gradient of ϕ, $D^2\phi$ denotes the Hessian, and sgn denotes the signature of a matrix, i.e., the number of positive eigenvalues minus the number of negative ones.

B.1. Stationary-phase analysis of (47)

To obtain (74), we need the Hessian

$$D^2\phi = \begin{pmatrix} D_\mu^2\phi & 0 \\ 0 & D_\eta^2\phi \end{pmatrix}, \tag{B.2}$$

where

$$D_\mu^2\phi = \begin{pmatrix} a_{11} & a_{12} \\ a_{12} & a_{22} \end{pmatrix}, \tag{B.3}$$

with the a computed from (55) to be

$$\begin{aligned} a_{ii} &= \frac{1}{\omega c}\left[\left(H - x_3^0\right)\left(\frac{1}{\tilde\mu_\infty} + \frac{\tilde\mu_i^2}{\omega^2(\tilde\mu_\infty)^3}\right) + (\gamma_3(s) - H)\left(\frac{1}{\tilde\mu_3^+} + \frac{\tilde\mu_i^2}{\omega^2\left(\tilde\mu_3^+\right)^3}\right)\right], \\ a_{12} &= \frac{\tilde\mu_1\tilde\mu_2}{\omega^3 c_0}\left(\frac{x_3^0 - H}{\tilde\mu_\infty^3} + \frac{\gamma_3(s) - H}{\left(\tilde\mu_3^+\right)^3}\right), \end{aligned} \tag{B.4}$$

and $D^2_\eta\phi$ is defined similarly. We note that a_{11} and a_{22} are both positive. Some algebra shows that the determinant of $D^2_\mu\phi$ is

$$\begin{aligned}\left|D^2_\eta\phi\right| = a_{11}a_{22} - a^2_{12} = \frac{1}{(\omega^3 c_0)^2}\Bigg[&\left(\frac{H - x^0_3}{(\tilde{\mu}_\infty)^3}\right)^2 \omega^2\tilde{\mu}^2_\infty\left(\omega^2\tilde{\mu}^2_\infty + |\tilde{\boldsymbol{\mu}}_T|^2\right)\\ &+\left(\frac{\gamma_3(s) - H}{\left(\tilde{\mu}^+_3\right)^3}\right)^2 \omega^2\left(\tilde{\mu}^+_3\right)^2(\omega^2(\tilde{\mu}_3)^2 + |\tilde{\boldsymbol{\mu}}_T|^2)\\ &+\left(\frac{H - x^0_3}{(\tilde{\mu}_\infty)^3}\right)\left(\frac{\gamma_3(s) - H}{\left(\tilde{\mu}^+_3\right)^3}\right)\left(\omega^2\tilde{\mu}^2_\infty\left(\omega^2\left(\tilde{\mu}^+_3\right)^2 + |\tilde{\boldsymbol{\mu}}_T|^2\right)\right.\\ &\left.+\omega^2\left(\tilde{\mu}^+_3\right)^2(\omega^2(\tilde{\mu}_\infty)^2 + |\tilde{\boldsymbol{\mu}}_T|^2)\right)\Bigg],\end{aligned} \tag{B.5}$$

which can be factored as shown in (76). We note that it is positive.

The eigenvalues of $D^2_\mu\phi$ are

$$\lambda_\pm = \frac{1}{2}\left[(a_{11} + a_{22}) \pm \sqrt{(a_{11} + a_{22})^2 - 4\left(a_{11}a_{22} - a^2_{12}\right)}\right]. \tag{B.6}$$

Since the determinant $a_{11}a_{22} - a^2_{12}$ is positive, the square root on the right-hand side of (B.6) is less than $|a_{11}+a_{22}|$, which means that the eigenvalues are both positive. Therefore the signature $\mathrm{sgn}D^2_\mu\phi$ is 2 and the signature $\mathrm{sgn}D^2\phi$ is 4, which implies that $\exp[\mathrm{i}\pi\,\mathrm{sgn}(D^2\phi)/4] = -1$. It is this minus sign that appears in front of (74).

Appendix C. Proof of proposition 5

First, we show as follows that $(s, \boldsymbol{\mu}_T, \tau)$ is a global coordinate system on Λ'. From examination of (77), we see that the only questions are whether t and $\boldsymbol{x}_T$ are uniquely and smoothly determined by knowledge of $(s, \boldsymbol{\mu}_T, \tau)$. With the help of (54), we rewrite the t equation of (77) as

$$t = \frac{2}{c_0}\left[\boldsymbol{\mu}_T \cdot (\boldsymbol{\gamma}_T(s) - \boldsymbol{x}_T) + \mu_\infty\left(H - x^0_3\right) + \mu^+_3(\gamma_3(s) - H)\right], \tag{C.1}$$

which expresses t in terms of s, $\boldsymbol{\mu}_T$ and $\boldsymbol{x}_T$. To see that $\boldsymbol{x}_T$ is determined by s and $\boldsymbol{\mu}_T$, we combine the two equations of (65) as $\boldsymbol{\gamma}_T(s) - \boldsymbol{x}_T = (R/r)\boldsymbol{\mu}_T$. Since R/r is given by (66) and from (65) we have that $r = |\boldsymbol{\mu}_T|$, R/r is in fact a function only of s and $\boldsymbol{\mu}_T$. We denote this function by $R/r = \rho(s, |\boldsymbol{\mu}_T|)$; we can thus write

$$\boldsymbol{\gamma}_T(s) - \boldsymbol{x}_T = \rho(s, |\boldsymbol{\mu}_T|)\boldsymbol{\mu}_T. \tag{C.2}$$

Solving (C.2) for $\boldsymbol{x}_T$ gives an explicit expression for $\boldsymbol{x}_T$ in terms of s and $\boldsymbol{\mu}_T$. Thus we see that $(s, \boldsymbol{\mu}_T, \tau)$ is a global coordinate system on Λ'.

The projection P maps a point on Λ', which is now specified by $(s, \boldsymbol{\mu}_T, \tau)$, to $(s, t; \sigma, \tau)$, where all variables are related by (77). To check that P is globally injective (one-to-one), we need to check that knowledge of $(s, t; \sigma, \tau)$ uniquely determines $\boldsymbol{\mu}_T$.

For a given position $\boldsymbol{\gamma}(s)$ and given travel time t, we see from symmetry that the corresponding set of possible $\boldsymbol{x}_T$ must be a circle on the plane x^0_3. For a given σ, the corresponding $\boldsymbol{x}$ have the property that $\sigma/(2k)$ is the cosine of the angle between the take-off direction $\boldsymbol{\mu}^+(s, \boldsymbol{x})$ and the flight direction $\dot{\boldsymbol{\gamma}}(s)$. On the plane $x_3 = x^0_3$, the set of such $\boldsymbol{x}_T$ forms two line segments making equal angles with the direction $\dot{\boldsymbol{\gamma}}_T(s)$. By assumption 8,

only one of these line segments corresponds to points of Λ'. This line segment intersects the constant-travel-time circle in one and only one point $\boldsymbol{x}_T$; $\boldsymbol{x}_T$ in turn determines $\boldsymbol{\mu}_T$. This shows that P is globally injective.

To check the injectivity of the derivative mapping

$$DP = \begin{pmatrix} \partial_s s & \partial_{\mu_1} s & \partial_{\mu_2} s & \partial_\tau s \\ \partial_s t & \partial_{\mu_1} t & \partial_{\mu_2} t & \partial_\tau t \\ \partial_s \sigma & \partial_{\mu_1} \sigma & \partial_{\mu_2} \sigma & \partial_\tau \sigma \\ \partial_s \tau & \partial_{\mu_1} \tau & \partial_{\mu_2} \tau & \partial_\tau \tau \end{pmatrix} = \begin{pmatrix} 1 & 0 & 0 & 0 \\ \partial_s t & \partial_{\mu_1} t & \partial_{\mu_2} t & \partial_\tau t \\ \partial_s \sigma & \partial_{\mu_1} \sigma & \partial_{\mu_2} \sigma & \partial_\tau \sigma \\ 0 & 0 & 0 & 1 \end{pmatrix}, \tag{C.3}$$

we need only compute the 2×2 submatrix in the centre. We calculate easily

$$\frac{\partial \sigma}{\partial \mu_j} = 2k\dot{\gamma}_j(s). \tag{C.4}$$

To compute $\partial t/\partial \boldsymbol{\mu}_T$, we use (C.2) to write the term $\mu_T \cdot (\gamma_T(s) - \boldsymbol{x}_T)$ appearing in (C.1) as $\tilde{\rho}(s, |\boldsymbol{\mu}_T|) = \rho(s, |\boldsymbol{\mu}_T|)|\boldsymbol{\mu}_T|^2$. We can now easily calculate the derivative

$$\frac{\partial t}{\partial \mu_j} = \frac{2}{c_0}\left[\frac{\tilde{\rho}'(s, |\boldsymbol{\mu}_T|)}{|\boldsymbol{\mu}_T|}\mu_j + \frac{\mu_j}{\mu_\infty}\left(H - x_3^0\right) + \frac{\mu_j}{\mu_c^+}(\gamma_3 - H)\right], \tag{C.5}$$

where the prime on $\tilde{\rho}$ denotes its derivative with respect to the second variable. Since $\nabla_{\mu_T} t \propto \boldsymbol{\mu}_T \propto \boldsymbol{\gamma}_T - \boldsymbol{x}_T$ is never collinear with $\nabla_{\mu_T}\sigma \propto \dot{\boldsymbol{\gamma}}_T$, DP has full rank.

References

[1] Albanese R A, Medina R L and Penn J W 1994 Mathematics, medicine, and microwaves *Inverse Problems* **10** 995–1007

[2] Beylkin G and Burridge R 1990 Linearized inverse scattering problems in acoustics and elasticity *Wave Motion* **12** 15–52

[3] Beylkin G 1985 Imaging of discontinuities in the inverse scattering problem by inversion of a causal generalized Radon transform *J. Math. Phys.* **26** 99–108

[4] Bleistein N and Handelsman R A 1986 *Asymptotic Expansions of Integrals* (New York: Dover)

[5] Bleistein N, Cohen J K and Stockwell J W 2000 *The Mathematics of Multidimensional Seismic Imaging, Migration, and Inversion* (New York: Springer)

[6] Brown G S and Curry W J 1982 A theory and model for wave propagation through foliage *Radio Sci.* **17** 1027–36

[7] Cheney M 2001 A mathematical tutorial on synthetic aperture radar *SIAM Rev.* **43** 301–12

[8] Cheney M and Isaacson D 1995 Inverse problems for a perturbed dissipative half-space *Inverse Problems* **11** 865–88

[9] Cutrona L J 1990 Synthetic aperture radar *Radar Handbook* 2nd edn ed M Skolnik (New York: McGraw-Hill)

[10] Duistermaat J J 1996 *Fourier Integral Operators* (Boston, MA: Birkhauser)

[11] Ding K H 2003 Private communication

[12] Egorov I 1999 Second forerunners in reflection and transmission data *J. Opt. A: Pure Appl. Opt.* **1** 51–9

[13] Elachi C 1987 *Spaceborne Radar Remote Sensing: Applications and Techniques* (New York: IEEE)

[14] Franceschetti G and Lanari R 1999 *Synthetic Aperture Radar Processing* (New York: CRC Press)

[15] Fung A K and Ulaby F T 1978 A scatter model for leafy vegetation *IEEE Trans. Geosci. Electron.* **16** 281–6

[16] Franchois A, Pineiro Y and Lang R H 1998 Microwave permittivity measurements of two conifers *IEEE Trans. Geosci. Remote Sens.* **36** 1384–95

[17] Fisher S E, Weile D S and Michielssen E 1999 Pareto genetic algorithm design of log-periodic monopole arrays mounted on realistic platforms *J. Electromagn. Waves Appl.* **13** 571–98

[18] Gustavsson A, Frölind P-O, Hellsten H, Jonsson T, Larsson B, Stenström G and Ulander L M H 1998 Development and operation of the FOA CARABAS HF/VHF-SAR system *Proc. 4th Int. Workshop on Radar Polarimetry (Nantes, France, 13–17 July 1998)*

[19] Grigis A and Sjöstrand J 1994 *Microlocal Analysis for Differential Operators: An Introduction (London Mathematical Society Lecture Note Series* vol 196*)* (Cambridge: Cambridge University Press)

[20] Guillemin V and Sternberg S 1979 *Geometric Asymptotics* (Providence, RI: American Mathematical Society)

[21] Herman G T, Tuy H K, Langenberg K J and Sabatier P C 1988 *Basic Methods of Tomography and Inverse Problems* (Phildelphia, PA: Hilger)
[22] Hellsten H, Ulander L M H, Gustavsson A and Larsson B 1996 Development of VHF CARABAS II SAR *SPIE Proc.* **2747** 48–60
[23] Jackson J D 1962 *Classical Electrodynamics* 2nd edn (New York: Wiley)
[24] Kong J A 1986 *Electromagnetic Wave Theory* (New York: Wiley)
[25] Karlsson A and Kristensson G 1992 Constitutive relations, dissipation and reciprocity for the Maxwell equations in the time domain *J. Electromagn. Waves Appl.* **6** 537–51
[26] Karlsson A and Rikte S 1998 The time-domain theory of forerunners *J. Opt. Soc. Am.* A **15** 487–502
[27] Lewis R M 1965 Asymptotic theory of wave-propagation *Arch. Ration. Mech. Anal.* **20** 191–250
[28] Langenberg K J, Brandfass M, Mayer K, Kreutter T, Brüll A, Felinger P and Huo D 1993 Principles of microwave imaging and inverse scattering *EARSeL Adv. Remote Sens.* **2** 163–86
[29] Lou Y 2002 Review of the NASA/JPL airborne synthetic aperture radar system *Geoscience and Remote Sensing Symp. IGARSS '02, IEEE International (June 2002)* vol 3 pp 24–8
[30] Milton G W, Eyre D J and Mantese J V 1997 Finite frequency range Kramers–Kronig relations: bounds on the dispersion *Phys. Rev. Lett.* **79** 3062–4
[31] Matzler C 1994 Microwave (1–100 GHz) dielectric model of leaves *IEEE Trans. Geosci. Remote Sens.* **32** 947–9
[32] Matzler C and Sume A 1989 Microwave radiometry of leaves *Microwave Radiometry and Remote Sensing Applications* ed P Pampaloni (Utrecht: VSP) pp 133–48
[33] Newton R G 1966 *Scattering Theory of Waves and Particles* (New York: Springer)
[34] Nilsson S 1997 Application of fast backprojection techniques for some inverse problems of integral geometry *Linköping Studies in Science and Technology, Linköping University Dissertation* No 499
[35] Nolan C J 2000 Scattering near a fold caustic *SIAM J. Appl. Math.* **61** 659–72
[36] Nolan C J and Cheney M 2002 Synthetic aperture inversion *Inverse Problems* **18** 221–36
[37] Nolan C J and Cheney M 2002 Synthetic aperture inversion for non-flat topography *Proc. 4th European Conf. on Synthetic Aperture Radar* (Berlin: VDE GMBH)
[38] Nolan C J and Cheney M 2004 Microlocal analysis of synthetic aperture radar imaging *J. Fourier Anal. Appl.* **10** at press
[39] Nolan C J and Symes W W 1997 Global solution of a linearized inverse problem for the acoustic wave equation *Commun. Partial Diff. Eqns* **22** 919–52
[40] Oughstun K E and Sherman G C 1994 *Electromagnetic Pulse Propagation in Causal Dielectrics* (New York: Springer)
[41] Roberts T M and Petropoulos P G 1996 Asymptotics and energy estimates for electromagnetic pulses in dispersive media *J. Opt. Soc. Am.* A **13** 1204–17
[42] Reed M and Simon B 1975 *Fourier Analysis, Self-Adjointness, Methods of Modern Mathematical Physics* vol 2 (New York: Academic)
[43] Treves F 1975 *Basic Linear Partial Differential Equations* (New York: Academic)
[44] Treves F 1980 *Introduction to Pseudodifferential and Fourier Integral Operators* vol I and II (New York: Plenum)
[45] Thomas R E and Huang J 1998 Ultra-wideband UHF microstrip array for GeoSAR applciation *IEEE Antennas and Propagation Society Int. Symp. (21–26 June 1998)* vol 4 pp 2096–9
[46] Therrien C W 1992 *Discrete Random Signals and Statistical Signal Processing* (Englewood Cliffs, NJ: Prentice-Hall)
[47] Ulander L M H, Hellsten H and Stenström G 2003 Synthetic-aperture radar processing using fast factorised backprojection *IEEE Trans. on Aerospace and Electronic Systems* **39** 760–76
[48] Ulaby F T and El-Rayes M A 1987 Microwave dielectric spectrum of vegetation: Part II. Dual-dispersion model *IEEE Trans. Geosci. Remote Sens.* **25** 550–7
[49] Ulander L M H and Hellsten H 1999 Low-frequency ultra-wideband array-antenna SAR for stationary and moving target imaging *Conf. Proc. SPIE 13th Ann. Int. Symp. on Aerosense (Orlando, FL, Apr. 1999)*
[50] Wheeler K and Hensley S 2000 The GeoSAR airborne mapping system *Record of the IEEE 2000 Int. Radar Conf. (7–12 May 2000)* pp 831–5
[51] Xiong Z and Tripp A C 1997 Ground-penetrating radar responses of dispersive models *Geophysics* **62** 1127–31
[52] Ziomek L J 1985 *Underwater Acoustics: A Linear Systems Theory Approach* (Orlando, FL: Academic)